CHALMERS

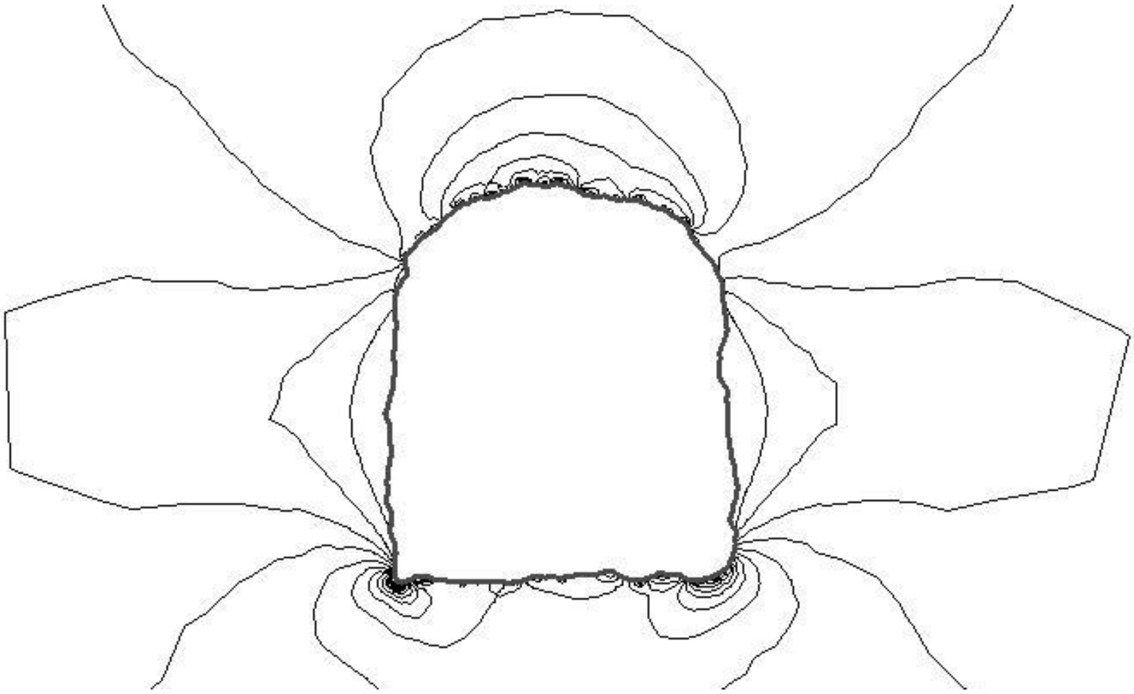

Support design for deposition tunnels

A case study of the TASS tunnel in Äspö Hard Rock Laboratory

Master of Science Thesis in the Master's Programme Geo and Water Engineering

HENRIK ITTNER

Department of Civil and Environmental Engineering
Division of GeoEngineering

Engineering Geology Research Group

CHALMERS UNIVERSITY OF TECHNOLOGY
Göteborg, Sweden 2011

Master's Thesis 2011:87

MASTER'S THESIS 2011:87

Support design for deposition tunnels

A case study of the TASS tunnel in Äspö Hard Rock Laboratory

Master of Science Thesis in the Master's Programme Geo and Water Engineering

HENRIK ITTNER

Department of Civil and Environmental Engineering
Division of GeoEngineering
Engineering Geology Research Group
CHALMERS UNIVERSITY OF TECHNOLOGY

Gothenburg, Sweden 2011

Support design for deposition tunnels
A case study of the TASS tunnel in Äspö Hard Rock Laboratory
Master of Science Thesis in the Master´s Programme Geo and Water Engineering
HENRIK ITTNER

Examensarbete / Institutionen för bygg- och miljöteknik,
Chalmers tekniska högskola 2011:87

Department of Civil and Environmental Engineering
Division of GeoEngineering
Engineering Geology Research Group
Chalmers University of Technology
SE-412 96 Göteborg
Sweden
Telephone: + 46 (0)31-772 1000

Cover:
The induced principal stress σ_1 stress field in section 24,7 m. Read more in Chapter 5.2.

Chalmers Reproservice
Gothenburg, Sweden 2011

Support design for deposition tunnels
A case study of the TASS tunnel in Äspö Hard Rock Laboratory
Master of Science Thesis in the Master´s Programme Geo and Water Engineering
HENRIK ITTNER
Department of Civil and Environmental Engineering
Division of GeoEngineering
Engineering Geology Research Group
Chalmers University of Technology

ABSTRACT

After interim storage the spent fuel from nuclear power plants in Sweden will be enclosed in copper canisters and placed in large, vertical boreholes in a system of deposition tunnels at a depth of 450 m in the bedrock (KBS-3 method).

A working environment risk for personnel working in the deposition tunnels are gravity or stress induced block falls. This risk could be reduced or avoided by supporting the rock mass in locations where block falls are most likely to occur. This thesis assesses the rock supporting alternatives maintenance scaling, spray concrete and wire mesh in limited sections. The evaluation includes numerical stress simulations, geological mapping and documentation of the construction process of rock support.

The TASS tunnel in Äspö Hard Rock Laboratory has similar geometry to the deposition tunnels which makes it suitable for a tunnel support test project. The results of the production of the spray concrete sections have shown to be satisfactory. It was possible to smoothen the contour and to fill overbreak areas by gradually decrease the thickness of the layer. The results from the production of wire mesh were also satisfactory. The mesh was easy to apply and has a good contact to the rock.

There should however be no risk for large scale spalling or crack initiation as the modeled values of induced stress generally are lower than the crack and spalling initiation limits of the rock. Stress induced block falls can therefore be considered to be limited in size. Rough surfaces, resulting in extreme stress values are most efficient reinforced with spray concrete as the contact with the rock is better than with a wire mesh.

Depending on the often time consuming work steps, the production of wire mesh have higher production costs compared to spray concrete. Thus the use of wire mesh is questionable since it does not have technical advantage over spray concrete.

The results from the theoretical evaluation correlate well to the support types assigned during mapping in the TASS tunnel. The reinforcement of deposition tunnels in the repository for spent nuclear fuel should focus on the areas with the most documented problems, i.e. the sections in the ends of the blast rounds. Support for those sections should be considered based on deviations in geometry and density of geological fractures. The recommended rock support alternative is spray concrete as it gives a better result with less use of recourses.

Key words: Deposition tunnel, Rock support, Spray concrete, wire mesh, Numerical stress simulation, Rock stresses, Geological mapping.

Design av bergförstärkning för deponeringstunnlar
En fallstudie av TASS-tunneln i Äspölaboratoriet
Examensarbete inom Mastersprogrammet Geo and Water Engineering
HENRIK ITTNER
Institutionen för bygg- och miljöteknik
Avdelningen för Geologi och geoteknik
Forskargrupp Geologi
Chalmers tekniska högskola

SAMMANFATTNING

Efter mellanlagring kommer det använda kärnbränslet från svenska kärnkraftverk att kapslas in i kopparkapslar och placeras i vertikala borrhål i ett system av deponeringstunnlar på 450 meters djup (KBS-3 metoden).

En arbetsmiljörisk för personer som arbetar i deponeringstunnlarna är gravitationsdrivna eller spänningsinducerade blockutfall. Den här risken kan undvikas eller minimeras om bergmassan förstärks i de sektioner där utfall är mest sannolikt. I detta examensarbete undersökes bergförstärkningsalternativen selektiv nätning och sprutbetong samt underhållskrotning. I utvärderingen ingick numerisk spänningssimulering, geologisk kartering och dokumentation av byggprocessen för de olika förstärkningsalternativen.

TASS tunneln i Äspölaboratoriet har en geometri som liknar den hos de planerade deponeringstunnlarna i kärnbränsleförvaret och har därför visat sig lämpad för ett bergförstärkningstest. Resultaten från sprutbetongarbetet är tillfredställande. Det var möjligt att jämna ut konturen och att fylla områden med överberg genom att gradvis minska sprutbetongens tjocklek. Resultatet från nätningen är även de tillfredställande. Nätet var enkelt att applicera och har en god kontakt mot bergytan.

Det borde inte finnas någon risk för storskalig sprickinitiering eller spjälkning i bergmassan eftersom de inducerade spänningarna generellt är lägre än gränsvärdena. Spänningsinducerade utfall kan därför antas ha en begränsad storlek. Råa ytor som resulterar i extremvärden förstärks bäst med sprutbetong eftersom den ger en bättre kontakt mot bergytan än nätning.

Nätning har högre produktionskostnader än sprutbetong beroende på många manuella tidskrävande arbetsmoment. Det här ifrågasätter användandet av nät eftersom nätning inte har några uppenbara tekniska fördelar gentemot sprutbetong.

Resultaten från den teoretiska utvärderingen stämmer bra överens med vad de förstärkningstyper som föreslogs under karteringen av TASS tunneln. Förstärkningsarbetena i deponeringstunnlarna i det planerade slutförvaret bör fokusera på de sektioner där problemen antas vara störst, dvs. i slutet av sprängsalvorna. Förstärkningstyp bör beslutas efter konturens geometri och antalet geologiska sprickor. Sprutbetong är att föredra framför nätning eftersom det ger ett bättre resultat och en effektivare resursanvändning.

Nyckelord: Deponeringstunnel, Bergförstärkning, Sprutbetong, Nät, Numerisk spänningssimulering, Bergspänningar, geologisk kartering.

Contents

Handledarnas förord

Det här examensarbetet har fokuserat på att utvärdera olika förstärkningskoncept för tämligen små tunnlar i kristallin berggrund av hållfasthetsmässigt god kvalitet, motsvarande de deponeringstunnlar i SKB:s planerade slutförvar för högaktivt radioaktivt avfall. Analysarbetet har utgått ifrån befintliga och egen-insamlade data från Äspölaboratoriet. Fältarbetet har omfattat bergbesiktning samt uppföljning av bergförstärkning med olika typer av förstärkningselement.

Fallande sten är en viktig arbetsmiljöfråga i berganläggningar där människor vistas och hanteras vanligtvis med olika typer av bergförstärkning. I ett geologiskt djupförvar för använt kärnbränsle ställs dessutom speciella krav på utförandet av bergförstärkningen. För detta har en analysmetod utarbetats som förenar praktisk erfarenhet med teoretiska beräkningar för olika typer av förstärkningselement.

Slutsatserna från examensarbetet utgör ett värdefullt bidrag i SKB:s arbete med att fastställa ett förstärkningskoncept för deponeringstunnlar i slutförvaret för använt kärnbränsle, och kan vara tillämpbart för icke-publika undermarksanläggningar i liknande bergförhållanden. Examensarbetet är väl utfört och uppfyller kriterierna som ställs för civilingenjörsexamen vid Chalmers Tekniska Högskola.

Göteborg i juni 2011

Lars O. Ericsson

Handledare/ Examinator

Chalmers Tekniska Högskola

Stockholm i juni 2011

Rolf Christiansson

Handledare

Svensk Kärnbränslehantering AB

Preface

This master thesis has been carried out for the Swedish Nuclear Fuel and Waste Management Company, SKB, at the Department of Civil and Environmental Engineering, Division of GeoEngineering at Chalmers University of Technology. The thesis has been supervised by Rolf Christiansson (SKB). Examiner was Lars O. Ericsson (Chalmers University of Technology).

Many persons have contributed during the work with the thesis. I wish to thank Rolf Christiansson and Lars O. Ericsson for helpful support and guidance during the work progress. Further I wish to thank Per-Erik Söder (Vattenfall Power Consultant AB), Anders Ansell (Royal Institute of Technology) and Derek Martin (University of Alberta) for inspiration and help with information and understanding of tunneling technology and rock support. A special thank is directed to Pär Kinnbom (3D-innovation AB) for providing necessary input data to the project.

I also wish to thank all the staff at Äspö Hard Rock Laboratory, especially Torgny Söderman, Emil Lindgren and Jerry Mohs at Söderman Bergsprängning AB for helpful advises and words of wisdom.

Gothenburg June 2011

Henrik Ittner

1 Introduction

1.1 Background

The radioactive waste from nuclear power plants in Sweden is managed by the Swedish Nuclear Fuel and Waste Management Co, SKB. After interim storage the fuel will be placed in impermeable copper canisters and transported to a planned geological repository in the Forsmark area in Östhammar, Sweden, see Figure 1.1. The canisters will be stored in large, vertical boreholes in a system of deposition tunnels at a depth of 450 m in the bedrock. After deposition, the deposition tunnels will be backfilled with bentonite-clay and sealed with concrete plugs.

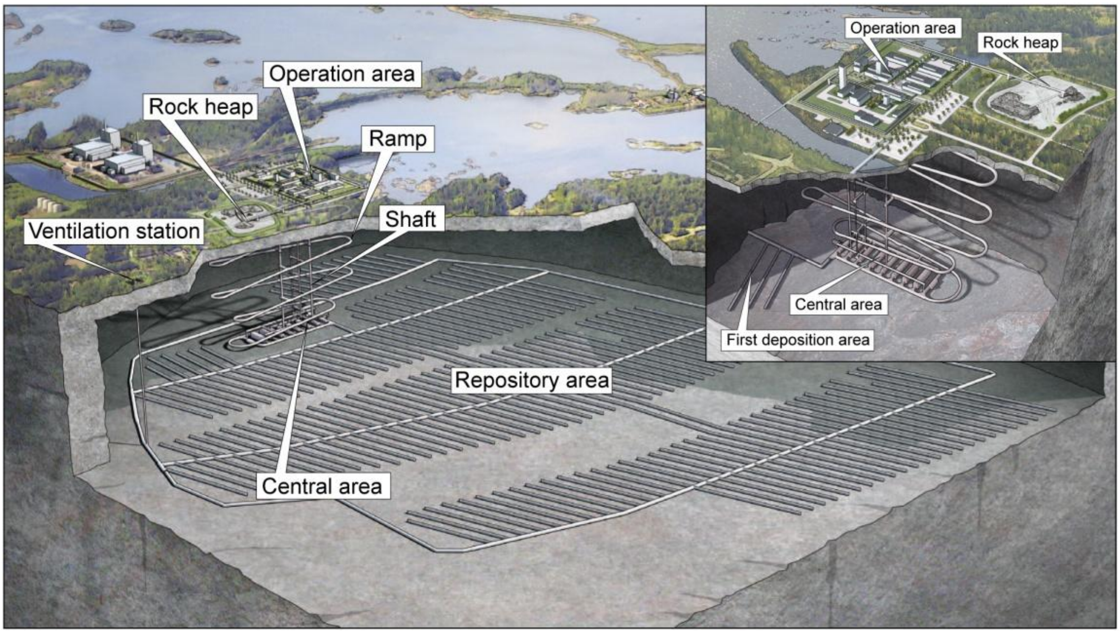

Figure 1.1 The planned geological repository in the Forsmark area in Östhammar. (SKB in Martin 2009).

The strategy of reinforcement for the deposition tunnels of the planned repository for spent nuclear fuel has until now only been studied in a general perspective. In the layout D2 it was estimated that due to the good rock quality in Forsmark and the short time before backfill there was no need for rock support in the deposition tunnels (Eriksson et al. 2009). There is however several reasons to investigate this further, one is the risk for temperature induced popping and spalling during work with heat producing machinery (Andersson and Söderhäll 2001). Another is gravity induced block falls, risking to impact vehicles or personal working underground (Martin 2009).

According to experience from Äspö Hard Rock Laboratory (HRL) the need for reinforcement is largest in the end of the blasting round. This is also were most of the maintenance scaling is conducted (Ittner 2010). Figure 1.2 shows the distribution of different causes for loose blocks scaled down from the tunnel roof in TASA, Äspö HRL.

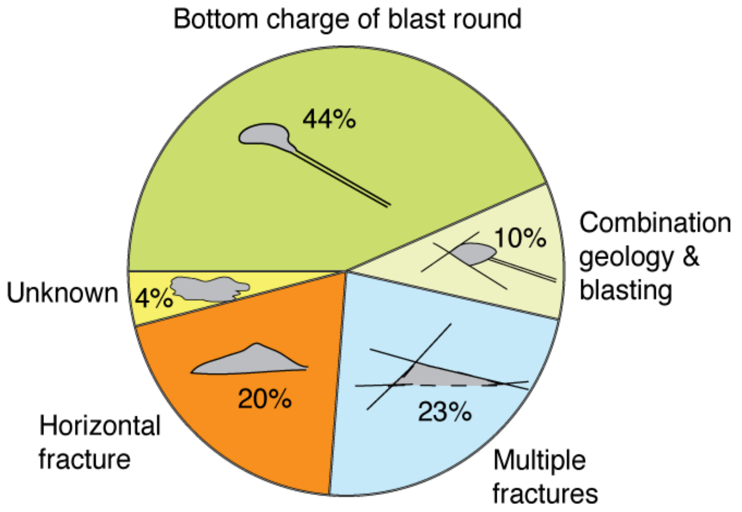

Figure 1.2 Distribution of causes for loose blocks scaled down from the tunnel roof in TASA, Äspö HRL (Martin 2009, modified from Ittner 2010).

These problems are related to the excavation method with drill and blast technology. As a result of the look-out angel required by the drilling rig, deviations from the theoretical tunnel contour are created. The deviations are largest in the end of the blast rounds, Figure 1.3. The geometrical deviation and heavier explosives used in the end of the blast rounds increases the risk for block falls in these areas.

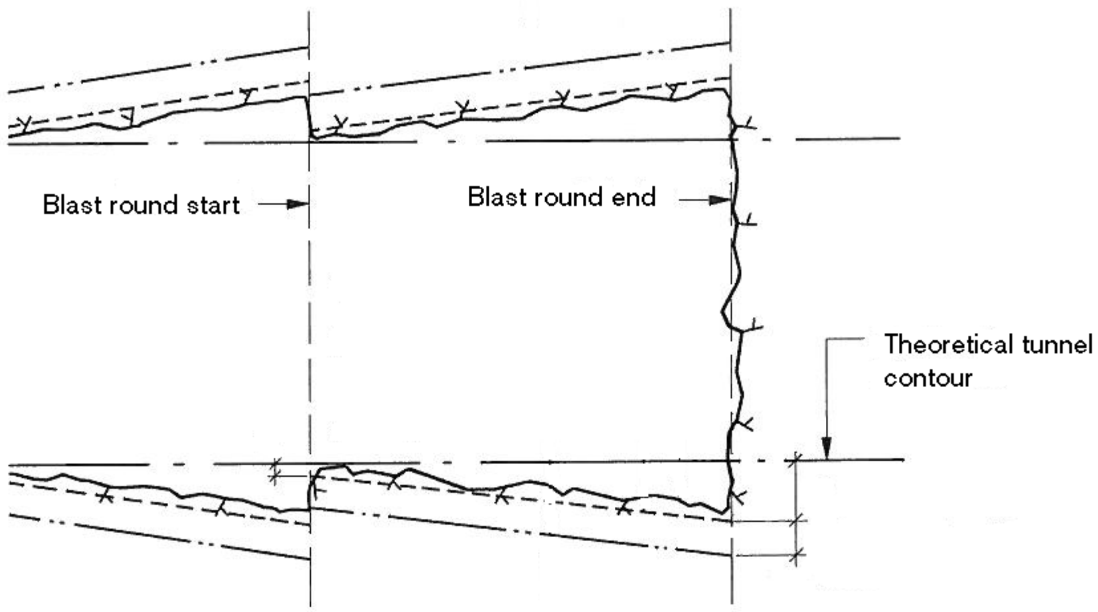

Figure 1.3 Plan of a tunnel section excvated with drill and blast techniqe. Note the deviation between excavated and theoretical contour (AB Svensk byggtjänst 1998, modified).

If those parts of the tunnel roof are supported, problems could be avoided or minimized. This requires a toolbox of support solutions depending on geology and quality of the blasting works.

Several alternatives for rock support are available. Possible solutions are sprayed concrete or wire mesh in combination with maintenance scaling.

The TASS tunnel, located in Äspö HRL at the -450 m level, was subjected to a rock support test during spring 2011. This included spray concrete and wire mesh in limited sections. The tunnel has a similar geometry to the deposition tunnels in the planned repository, which makes it suitable for a tunnel support test project. In later projects the tunnel will be used as a test tunnel for the backfill technology. This gives a good opportunity to test behavior of reinforcement in a deposition tunnel after deposition and backfill have been completed.

1.2 Objective

A safe working environment is important during construction and operation of the deposition tunnels in the repository for spent nuclear fuel. A possible danger for the personnel working in the deposition tunnels are gravity or stress induced block falls. This risk could be reduced or avoided by supporting the rock mass in locations were block falls are most likely to occur.

The aim of this master thesis was to develop and evaluate a toolbox of rock support solutions for deposition tunnels in massive crystalline bedrock. This was achieved by evaluation of the geological situation, construction costs and design of rock support in the TASS tunnel in Äspö HRL. A method of evaluation was developed based on Finite element analysis, analytical calculation methods and experience from mapping and construction works. The thesis focused on sprayed concrete and wire mesh in limited sections, their technical behavior and behavior during construction.

1.3 Scope of work

The work conducted in order to complete this thesis was fieldwork, a literature survey and analysis using numerical stress modeling. In addition available statistics from mapping and other documentation, for example construction costs and observations of the rock support installation during the construction have been evaluated. Based on this, a conceptual model for the TASS tunnel behavior has been developed. The numerical stress modeling was a part of the conceptual model. Figure 1.4 shows the sections of the tunnel were the need for rock support was evaluated.

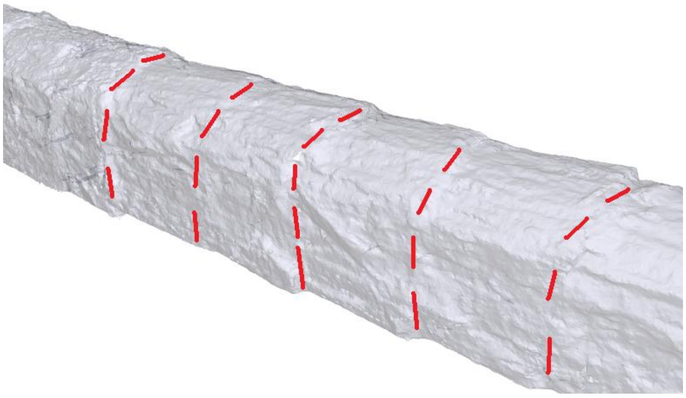

Figure 1.4 Laser scanned model of the TASS tunnel, the critical sections are marked red in the figure. Figure by Pär Kinnbom (modified).

The author conducted mapping of overbreak areas and evaluation of scaling records in the tunnel roof of the TASA access tunnel at Äspö HRL during 2009. The aim of the TASA project was to establish a block mass distribution for blocks scaled from the tunnel roof and abutments and to document the causes and location of scaling. Several of the conclusions and experiences from this project have been useful for this master thesis. The results from the TASA project are presented in the SKB report IPR-10-01.

The literature survey was compiled in order to form a basis for the finite element analysis of the TASS tunnel system behavior. It included studies of the in-situ stress situation at the -450 m level in Äspö HRL, the properties of the rock mass at the actual level and a compilation of field tests related to crack initiation and spalling. It also included properties, behavior and theory concerning rock support technology, focusing on spray concrete and wire mesh.

Several field works and site inspections were included in the frame of the master thesis. This included rock mechanical mapping of the TASS tunnel in February 2011. The mapping conducted during this field work formed the basis for a rock support test project for the TASS tunnel. Spray concrete works were performed by the contractor BESAB during the end of April and beginning of May 2011. And wire mesh works were conducted by Söderman Bergssprängning AB during may 2011. Site inspections were preformed during the construction works, in order to document the work and to obtain data for the analysis.

2 Site conditions

This chapter presents the site conditions. It includes a description of the case of study, in situ stresses and geological situation.

2.1 The TASS tunnel

In 1986 SKB decided to construct an underground Hard Rock Laboratory (HRL) in order to perform research in an environment similar to that of the planned deep repository for spent nuclear fuel. The tunnels were excavated in the area of Simpevarp in the north-eastern corner of the municipality of Oskarshamn, Sweden.

Johansson and Karlzén (2010) described the planning, documentation and excavation of the TASS tunnel.

From the end of 2007 until the end of 2008 SKB excavated the TASS-tunnel in Äspö HRL. TASS is an abbreviation where T=tunnel, AS=Äspö site and S=letter of ID. Figure 2.1 shows the underground part of Äspö HRL. The location of the TASS-tunnel is shown in the figure.

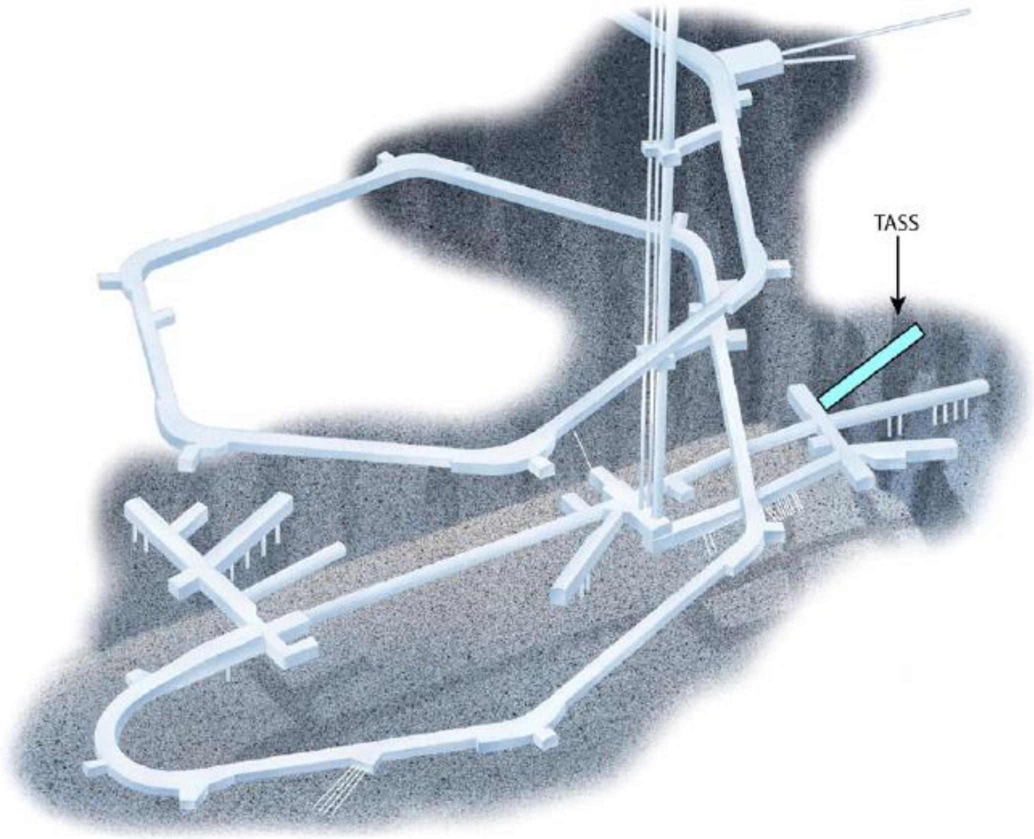

Figure 2.1 The underground part of Äspö HRL. The location of the TASS-tunnel is shown in the figure (Andersson and Malmtorp 2009).

The main purpose of the tunnel was to conduct a full scale test of grouting technology, using silica sol. Therefore the tunnel was driven in an area with water bearing fractures, suitable for testing grouting technology. The pre-investigations showed sets of water bearing, steep dipping fractures with a NW-NNW orientation (Andersson and Malmtorp 2009).

In addition to this different blasting and drilling techniques and explosives was tested in order to achieve a good contour and minimize damage to the surrounding rock mass.

With a length of approximately 80 m and a theoretical cross section of approximately 19 m^2 its dimensions are similar to a deposition tunnel of the planned repository in Forsmark. The tunnel was excavated at the 450 m level in 215.8° with reference Magnetic North. (Hardenby and Sigurdsson 2010)

2.1.1 Excavation of TASS

The backfill procedure and the risk for water leakage through damaged rock mass puts high demands on the geometry, contour and excavation damage zone (EDZ) for the deposition tunnels. Those demands were applied during the excavation of TASS. The aim was to accomplish the following demands for contour and overbreak (Johansson and Karlzén 2010):

1. The tunnel contour was not allowed to be smaller than the theoretical contour, i.e. 4,2 m.
2. The overbreak was not allowed to exceed 30 % in each blasting round.
3. No remaining rock inside the theoretical contour.
4. Deviation from theoretical contour in the end of blast rounds in the tunnel roof: 20 cm.
5. Deviation from theoretical contour in the end of blast rounds in the tunnel floor: 25 cm.

Demands for drilling, loading and blasting design were set after those demands.

The tunnel was excavated in stages with 2 to 4 rounds in each stage. In total 20 rounds were excavated in 6 stages. The deviation from theoretical contour in the end of blast rounds in the tunnel roof were changed after round 8 from 20 to 25 cm.

All of the demands were more or less successfully fulfilled. The small amount of remaining rock inside the theoretical contour could be removed with for example mechanical scaling. There is no significant difference in overbreak between 20 and 25 cm deviation from theoretical contour in the end of blast rounds, the volumes differ 1,5 %.

The project has been carefully planned in order to allow time for observation, reflection and feedback. This has resulted in a good quality of the excavated tunnel.

2.1.2 Backfill of KBS-3 deposition tunnels

Backfill of the deposition tunnels will be conducted with bentonite clay. A certain density per m^3 of the tunnel is chosen in order to prevent water leakage (Johansson and Karlzén 2010). Blocks of bentonite clay are stacked on each other and the remaining space between the blocks and the tunnel contour are filled with bentonite pellets. The canister will be placed in the deposition hole embedded by bentonite blocks. A schematic picture of a backfilled deposition tunnel is shown in Figure 2.2

It is desirable to minimize overbreak as the pellets cannot reach the same density as the bentonite blocks. Rock inside the theoretical contour will however complicate the work. Overbreak can also reduce the capacity of the bentonite to keep the canister from moving vertically if bentonite in the deposition hole expands before the backfill has reached saturation.

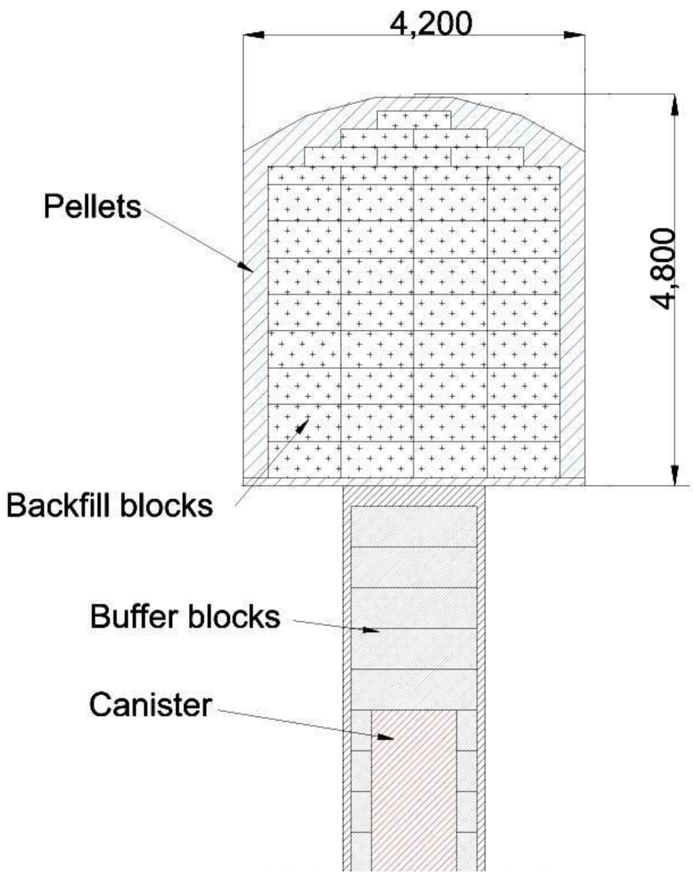

Figure 2.2 Schematic picture of a backfilled deposition tunnel (Johansson and Karlzén 2010).

2.2 Geology and rock stress

2.2.1 Geology of the Äspö area

The major parts of Precambrian bedrock of south-eastern Sweden belong to the so-called Transscandinavian Igneous Belt (TIB) which was formed during intense periods of magmatism during the Svecokarelian orogency. The geology in the Äspö-Simpevarp-Laxemar region is dominated by intrusive rocks of the TIB but the geological development of the region include periods of metamorphosis, resulting in both mineralogical, chemical and structural changes in the bedrock.

The dominating rock types found in the Äspö area are listed below. Note that the names for the rock types *Ärvö granite* and *Äspö diorite* have been reworked, these names are however still commonly used (Berglund et al. 2003):

- *Ärvö granite*: a medium grained, equigranular granite to granodiorite, including subordinate quartz monzodiorite.
- *Äspö diorite:* a medium-grained, sparsely to strongly porhyritic intrusive rock that varies in composition between granite and quartz diorite, including tonalitic, granodioritic, quartz monzonitic and quartz monzondioritic varieties.
- A grey, fine-grained, at places slightly porphyritic, intermediate rock.
- Dykes of fine-grained granite and pegmatite are frequently occurring.
- Mafic rocks. These are undifferentiated amphibolites, but most of them are considered to be genetically related to the granitoids and dioritoids of the TIB.

2.2.2 In-situ and induced stress

Kirsch (1898) presented an analytical solution for the stress distribution in a stressed elastic plate containing a circular hole.

Two types of stresses influence the rock mass around underground openings, primary and secondary. Primary or in-situ stresses are the stresses present in the bedrock before an underground opening is excavated. They are denoted in as σ_v, σ_{h1} and σ_{h2}. Secondary stresses or induced principal stresses are results of the excavation and compensate for the removed rock volume. They are denoted in order of magnitude as σ_1, σ_2 and σ_3. Figure 2.3 gives an overview of the stress situation around a circular opening.

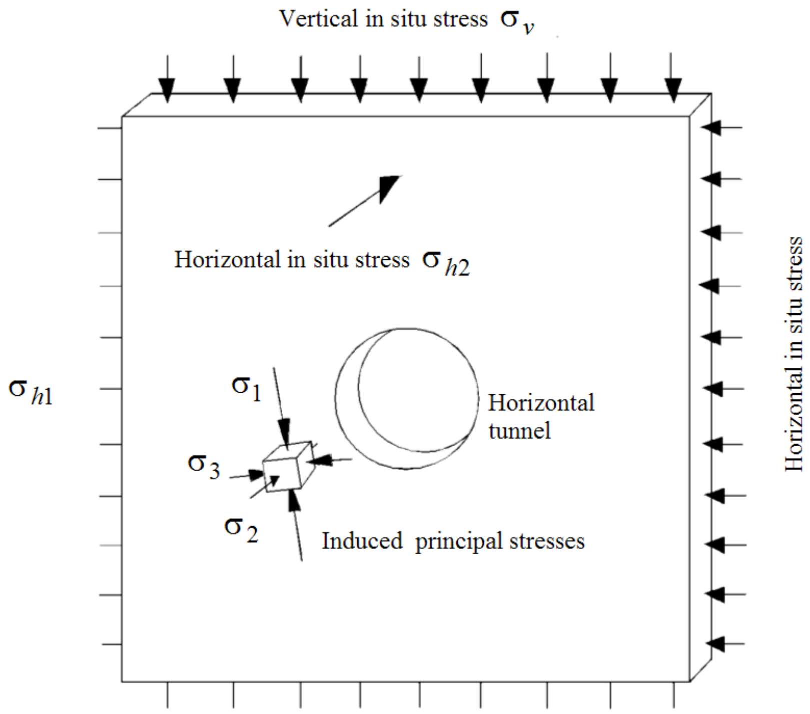

Figure 2.3 The stress field in a plate with a circular opening, after Kirsch (1898) in Hoek (2007).

The in-situ stress field in the Swedish bedrock is a result of several occurrences during the geological history, mainly tectonic events and isostatic uplift of the bedrock originating from the Pleistocene ice sheet (Lindblom 2010).

Based on focal mechanics, borehole breakout, overcoring methods and hydraulic fracturing the World Stress Map Project has completed a stress map of Scandinavia, Figure 2.4 The general orientation of major horizontal stresses in south western Sweden are approximately in a range of N130 to 150 based on this compilation

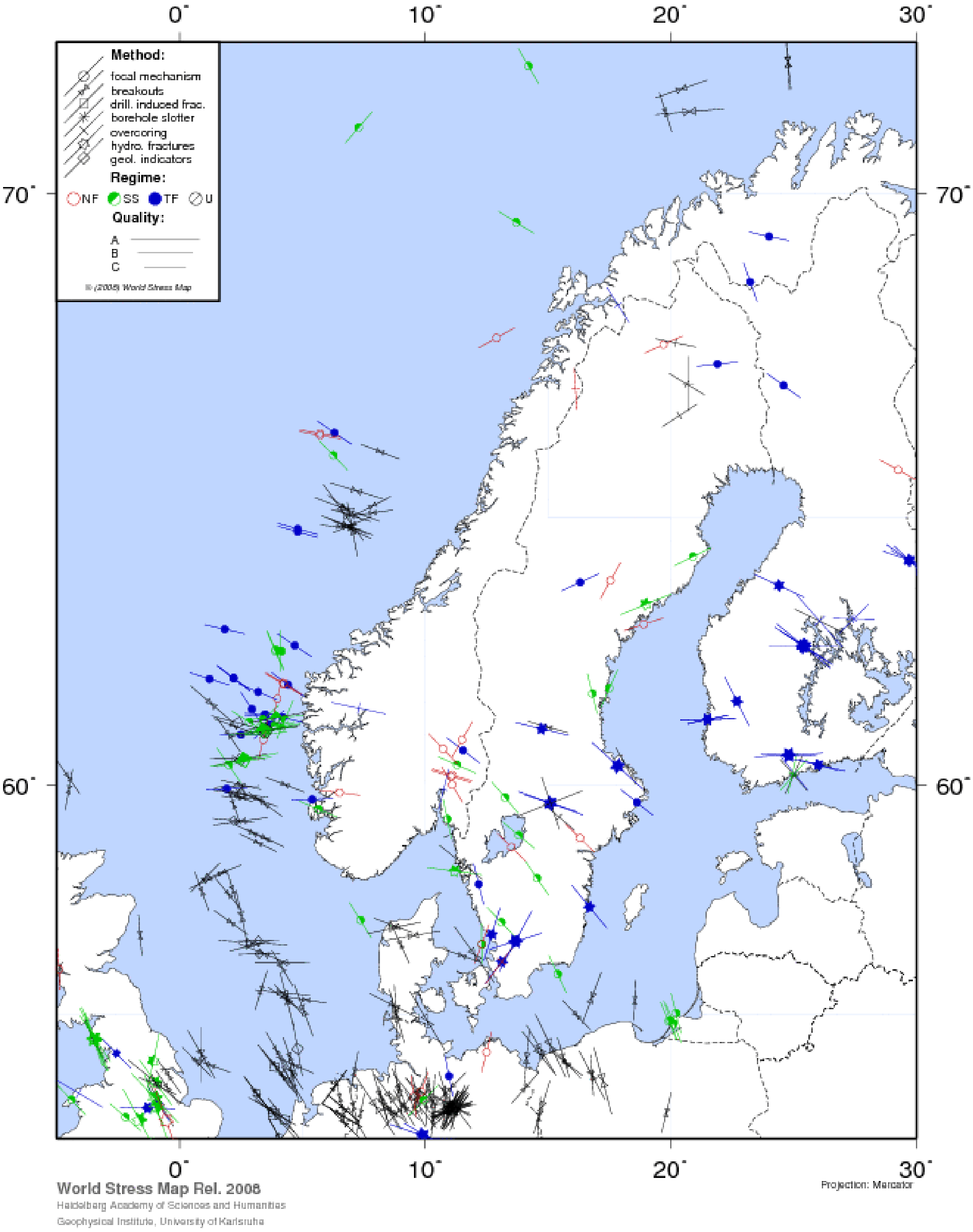

Figure 2.4 Stress map of Scandinavia with major horizontal stress orientations. Note the general orientation of major horizontal stresses in south western Sweden (world stress map) 2011-05-28

(http://dc-app3-14.gfz-potsdam.de/pub/stress_data/stress_data_frame.html).

2.2.3 Stress measurement methods

A major concern in rock mechanics is to estimate the magnitude and orientation of in-situ stresses. There are several techniques to estimate the in-situ stress state in a rock mass, including surface relief methods, borehole relief methods and hydraulic methods. It is also possible to estimate stress magnitudes through back analysis, based on deformation measurements during excavation (Ljunggren et al. 2003).

Ljunggren et al. (2003) gives an overview of rock stress measurement methods.Two of the most commonly used stress measuring methods in Scandinavia includes hydraulic and borehole relief methods. Examples of these methods are classical hydraulic fracturing, hydraulic tests on pre-existing fractures (HTPF), overcoring of measuring cells in pilot-holes and overcoring of borehole-bottom cells. However several other methods are also available.

2.2.4 Results of stress measurements from Äspö HRL

In 2001 several tests was carried out in the Äspö HRL in order to determine the in-situ stresses in the rock mass, this includes Deep Doorstopper Gauge System (DDGS), Borre Probe and Hydraulic Fracturing (HF). (Jansson and Stigsson 2002). Table 2.1 shows a summary of the results.

Table 2.1 Summary of the results from the measuring of the stresses in the vertical and horizontal borehole, at level –450 m (Jansson and Stigsson 2002).

Method	**Min horizontal stress [Mpa]**	**deviation ±**	**Max horizontal stress [Mpa]**	**deviation ±**	**Vertical stress [Mpa]**	**deviation**
DDGS, Vertical hole	22,2	1	36,7	2,6	-	-
HF, vertical hole	11	1	21,8	4,5	-	-
DDGS, horizontal hole	12,4	0	-	-	32,6	5,6
Borre Probe	10,2	2	25,8	3,5	18	8,8
HF, horizontal hole	11	1	-	-	19,8	1,6
Theoretical	-	-	-	-	12,2	0
Former measurements	10,5	3	21	5	15	4,5

Jansson and Stigsson (2002) gives the following conclusion for the stress state in the rock mass at the -455 m level in Äspö HRL:

“The minimum horizontal stress is between 10 and 13 MPa, which is lower than the theoretical vertical stress. The maximum horizontal stress is 24 ±5 MPa, most likely within the upper range. The vertical stress is between 15 and 20 MPa, most probably is this value only local due to the presence of a nearby fracture”

Table 2.2 presents a summary of the in situ stresses at the -455 m level. For σ_V the rounded theoretical value has been used.

Table 2.2 A summary of the in situ stresses at the -455 m level.

	σ_{h1}	σ_{h2}	σ_v
In situ stress [MPa]	30	13	13

2.3 Rock mass properties and influences of induced principle stress

2.3.1 Elastic properties of the rock mass in Äspö HRL

Andersson and Staub (2004) evaluated the rock mass properties for the rock types in the Äspö area in the frame of the Äspö Pillar Stability Experiment (APSE) in 5 core drillings in the TASQ tunnel. The mean values are shown in Table 2.3.

Table 2.3 Rock mass properties for the rock types in the Äspö area (Andersson and Staub 2004).

Rock type	**Young’s Modulus [GPa]**	**Poisson’s ratio [-]**	**Cohesion [MPa]**	**Friction angle [°]**	**Tensile strength [MPa]**
Diorite	55	0, 26	16,4 ± 3	41,4 ± 4	14,8

2.3.2 Crack initiation and spalling

Based on rock sample tests conducted in the frame of the APSE in 5 core drillings in the TASQ tunnel crack initiation stress was evaluated (Andersson and Staub 2004). The crack initiation and damage stress was evaluated from the volumetric stress/strain curves from uniaxial and triaxial tests and from the intensity of Acoustic Emission (AE) events recorded versus axial stress. The results are shown in Table 2.4.

Table 2.4 Crack initiation limit (Andersson and Staub 2004).

Method	**Strain curves**	**Acoustic Emission (AE)**
Crack initiation stress [MPa]	96,1 ± 12	121 ± 31,3
Crack damage stress [MPa]	201,8 ± 30,4	204 ±15,6

Spalling is a phenomenon similar to buckling that can occur in highly stressed massive brittle rock. The phenomenon is generally described in Bawden et al. (2000). A crack is formed and initiates parallel to the direction of the maximum compressive stress concentration. The failure then propagates orthogonal to the major principal stress direction until a slab of rock is detached. The process can lead to an instant detach of the rock slab or a gradually spalling. In both cases this can lead to damage or injury to personnel or machines working underground it they are impacted by a falling rock slab (Bawden et al. 2000).

Figure 2.5 shows spalling in the sidewalls of a borehole excavated in the frame of the Äspö Pillar Stability Experiment (APSE).

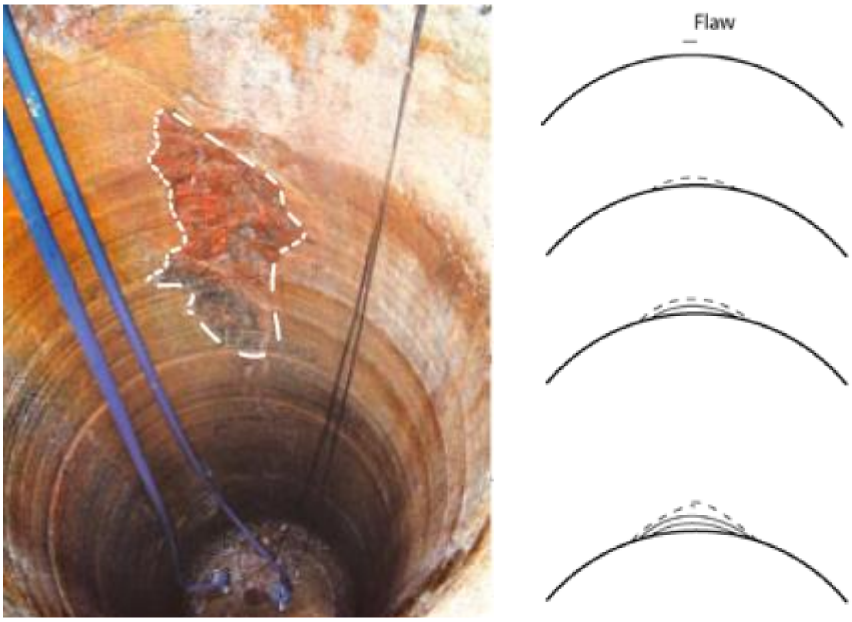

Figure 2.5 Left: spalling in the sidewalls of a borehole excavated in the frame of the Äspö Pillar Stability Experiment (APSE). The damaged area is indicated by a dashed white line. Right: The spalling process where the crack is initiated and gradually develops until a state of equilibrium is reached (Andersson 2007).

In the Äspö Pillar Stability Experiment (APSE), Spalling strength was measured in 21 points along a vertically drilled Ø1,75 m borehole subjected to a load from increased temperature (Andersson 2007). Two boreholes with the same diameter were drilled vertical into the tunnel floor, leaving a pillar of approximately 1 m width between them. The results are presented in Table 2.5.

Table 2.5 Spalling strength based on Andersson (2007).

	Mean value	**Standard deviation**
Spalling strength [MPa]	122	9

The results indicate that the spalling strength is affected by the rock type and by fractures. Test points located in green stone or close to pre-existing fractures showed lower spalling strength.

2.4 Mapping and documentation in the TASS tunnel

The TASS tunnel is well documented through pre-investigations and geological mapping conducted during and after the excavation works was completed. This chapter gives an overview of the mapping, relevant for the thesis, conducted in the TASS tunnel.

2.4.1 Pre-investigation and geological mapping

Before the start of the excavation a pre-investigation was conducted. This included three core-drillings, K10010B01, K10014B01 and K10016B01, drilled parallel to the tunnel direction. Two of them are located in the tunnel face and one in the rock mass of the right tunnel wall, see Figure 2.6.

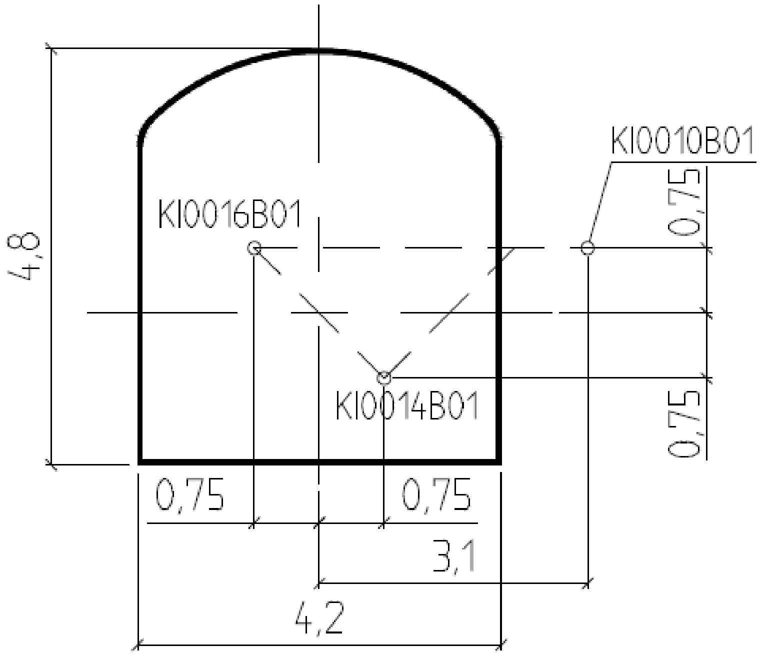

Figure 2.6 TASS tunnel theoretical profile and locations of the core-drillings, K10010B01, K10014B01 and K10016B01 (Andersson and Malmtorp 2009).

The drill cores showed sets of water bearing, steep dipping fractures with a NW-NNW orientation. Water flows of 20–60 l/min were measured for the first 100 meters of test drill holes (Andersson and Malmtorp 2009).

Figure 2.7 shows the RQD-values for the two diamond core drillings, drilled parallel to the tunnel direction into the tunnel face, before the start of the excavations (Andersson and Malmtorp 2009).

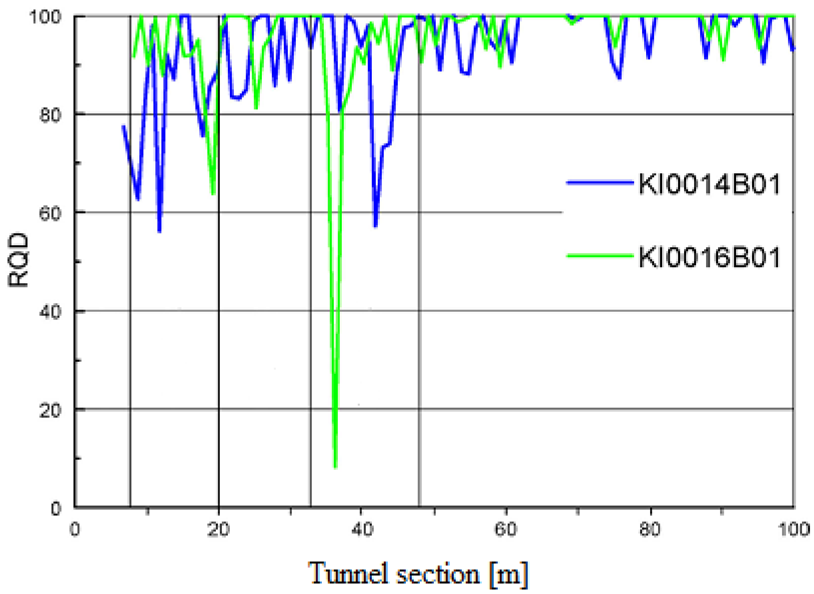

Figure 2.7 RQD-values for the two diamond core drillings drilled into the tunnel face. Compare with the fracture density in Figure 2.9. Modified from (Andersson and Malmtorp 2009).

A comprehensive geological mapping of the TASS-tunnel has been conducted by Hardenby and Sigurdsson (2010).

The following major items are registered during the mapping

- rock types
- rock boundaries/contacts
- alteration
- fractures
- deformation zones
- occurrence of water/water leakage
- Rock Mass Rating (RMR)

Normally, the cut-off for fractures is 1 m in length.

The report summarizes the results of the mapping together with the results from the Laser scanning, described in chapter 2.4.2, results of the mapping are in short:

Two main sets of fractures were identified in the TASS-tunnel:

1. East-west striking and steeply dipping. This fracture set dominates with a mean orientation of 097/86

2. Sub-horizontal to gently dipping with a more varying strike. This set may be divided into two sub-sets with the mean orientations 037/03 and 280/18 respectively

The Schmidt plot in Figure 2.8 depicts the orientation of all fractures mapped in the walls, roof, floor and current tunnel face.

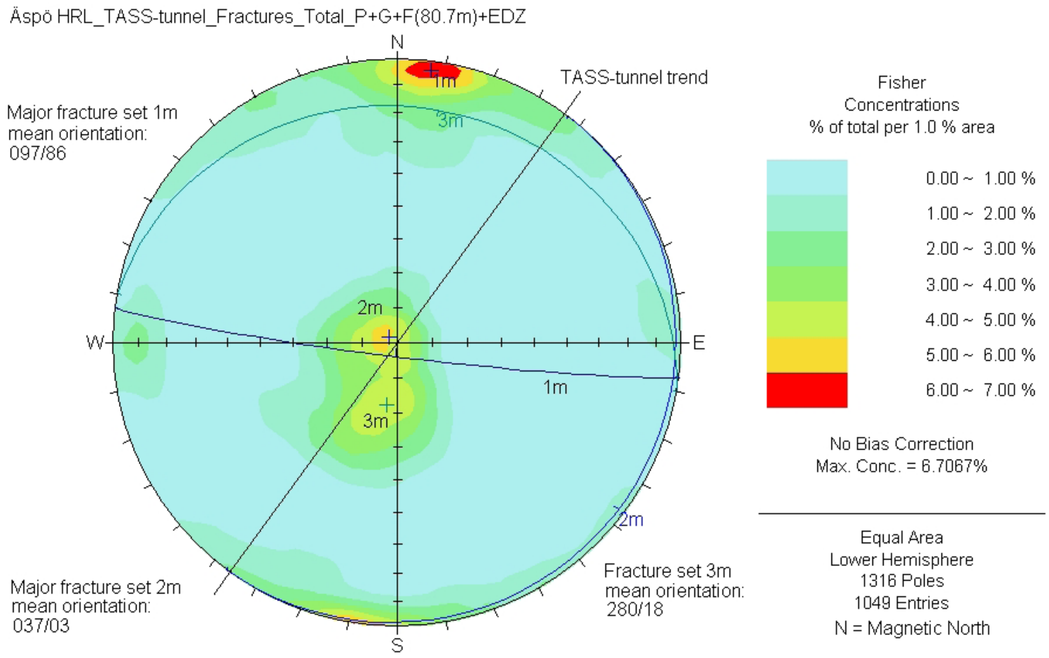

Figure 2.8 The Schmidt plot depicts the orientation of all fractures mapped in the walls, roof, floor and current tunnel face. The tunnel orientation is noted with a black line. Note the two main fracture sets. One east-west striking and steeply dipping and one Sub-horizontal to gently dipping with a more varying strike (Hardenby and Sigurdsson 2010).

Appendix A presents a geological map of the TASS tunnel with mapped geological fractures, rock types and rock contacts.

The dominating rock type in the tunnel is *Äspö diorite,* which constitutes some 90% of the rock mass. It is mostly mapped as fresh rock. Minor constituents of the rock mass are: fine-grained granite, hybrid rock, pegmatite, quartz veins/lenses and undifferentiated mafic rock.

2.4.2 Laser scanning

During 2008 and 2009 a full 3D laser scanning of the TASS tunnel was conducted. The scanning of the TASS-tunnel and some general principles of laser scanning are described by Hardenby and Sigurdsson (2010) and Johansson and Karlzén (2010). A second laser scanning was performed in May 2011.

The principle of laser scanning is that the scanner sends out infrared light that will spread in all directions as the scanner rotates. The scanner measures the distances to the surfaces that the infrared light it is reflected from based on the *travel time* of the beam or the *phase shift*, depending on the technology used. Based on this x, y and z coordinates for the surfaces are delivered by the scanner in a temporary coordinate system.

2.4.3 Geological fractures of the different blasting rounds

Based on the geological mapping conducted by Hardenby and Sigurdsson (2010) scan line mapping has been conducted in the end of the blasting rounds 6 to 20, Figure 2.9. The compiled statistics therefore only contains geological fractures longer then > 1 meter. The scan lines were placed 0,2 meter behind the rounded value of the start section of the next round. This means that the actual position can vary between 0,1 and 0,2 m behind the start of the next blast round. The start value for each section is based on Johansson and Karlzén, (2010). Appendix A contains the basis for the compiled statistics.

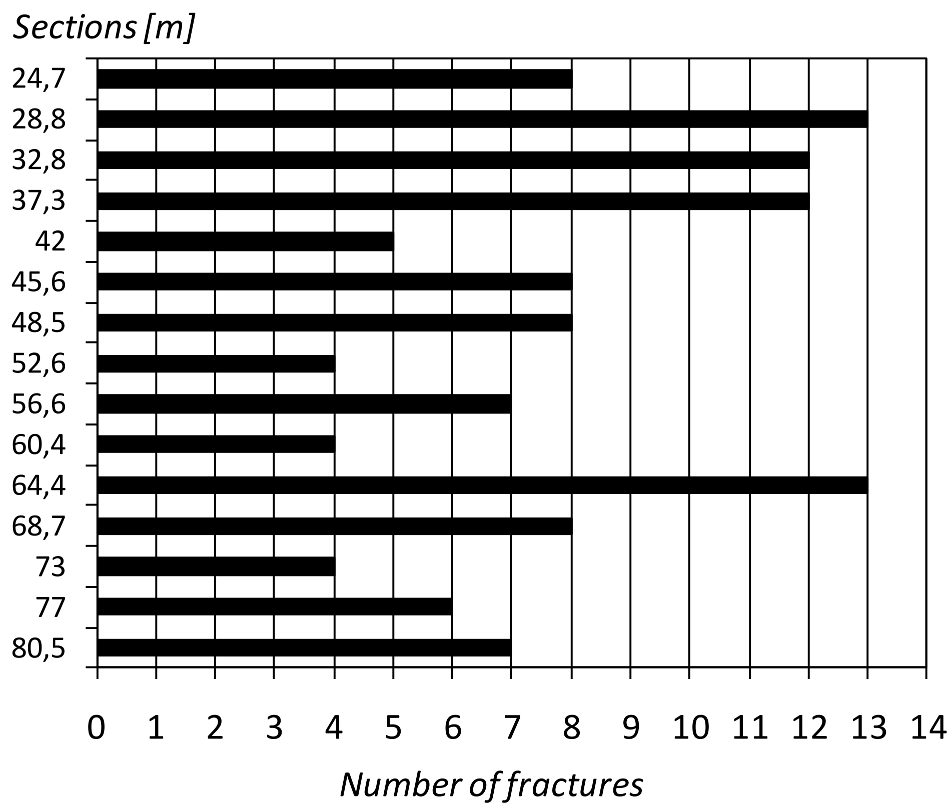

Figure 2.9 Number of geological fractures in the roof and abutment for each studied section. Note the high density of fractures in the sections 24,7 m to 37,3 m and compare with Figure 2.7.

2.4.4 Scaling statistics

The TASS tunnel has been subjected to maintenance scaling on a regular basis. During scaling occasions the mass of scaled rock material has been noted for each blasting round. It has also been noted were the scaling was conducted, i.e. right wall, left wall or roof/abutment. Figure 2.10 shows the mass of rock in each blasting round, scaled in the roof and abutment during the period august 2009 to June 2010. Note that the scaling is compiled for the whole section and not only for the blast round end, compare with map 3, *Maintenance scaling*, in appendix E.

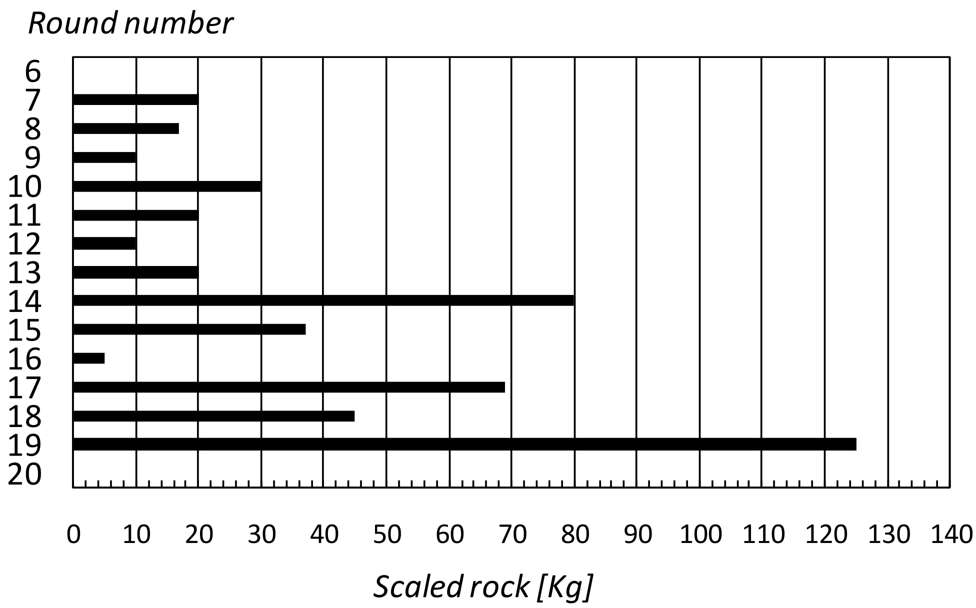

Figure 2.10 Maintenance scaling for each round scaled in the roof and abutment during the period august 2009 to June 2010. Compare with map 3, Maintenance scaling, in appendix E.

3 Rock support

This chapter gives an overview of spray concrete and mesh rock support technologies. The focus is on technologies intended to be used in the repository for spent nuclear fuel.

3.1 Rock bolts

Rock bolts can be used either systematic or as spot bolts to secure single unstable blocks. In the deposition tunnels grouted rock bolts will be used to secure larger blocks. This enables an approach were spray concrete and wire mesh can be more adequately designed.

3.2 Spray concrete

In order to construct a spray concrete reinforcement, concrete is sprayed onto a surface. If conducted in the right way, a high quality product can be constructed on uneven surfaces. The technology uses compressed air to reach high velocities up to 100 m/s, which compacts the concrete. Sprayed concrete can be reinforced with a steel mesh or with steel fibres to increase its ability to withstand strain and tensile failure (Lindblom 2010).

Spray concrete is used worldwide for support of underground constructions. Depending on the behaviour of the rock mass, a spray concrete lining will have different functions. There is a difference between underground constructions in hard and soft rock in this perspective, as in soft rock tunnelling the lining is allowed to deform before it is stopped by the support. Hard rock types are able to withstand the redistribution of stresses caused by the excavation to a much larger extent.

In hard rock tunnelling a spray concrete lining has the main function to stabilize potentially rotating or sliding key blocks. Stresses will however be induced and distributed into the spray concrete by small movements in the rock mass until a state of equilibrium has been reached (Holmgren 1979). This requires that further loosening of key blocks can be avoided.

3.2.1 Spray concrete subjected to punch load

Holmgren (1979) performed a large series of punch load tests on spray concrete slabs and arcs, from which the yielding steps could be identified. A summary of the results together with calculation strategies are presented in Holmgren (1992).

The most probable load case in scandinavian hard rock tunnelling is a loose block in the tunnel roof or abutment punching through the sprayed concrete layer, Figure 3.1

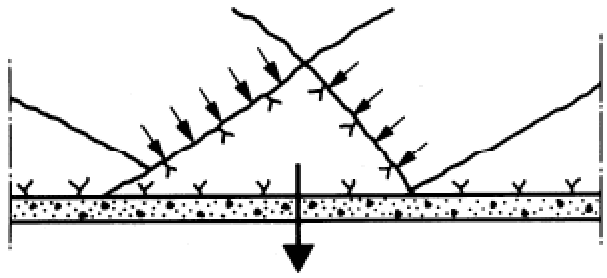

Figure 3.1 The assumed load case, a punch loaded spray concrete layer (Holmgren 1979).

A loose block punching through the spray concrete lining will, after the initial elastic state lead to adhesion cracking in the contact surface between spray concrete and rock. Continued loading will then cause flexural or shear cracking, Figure 3.2.

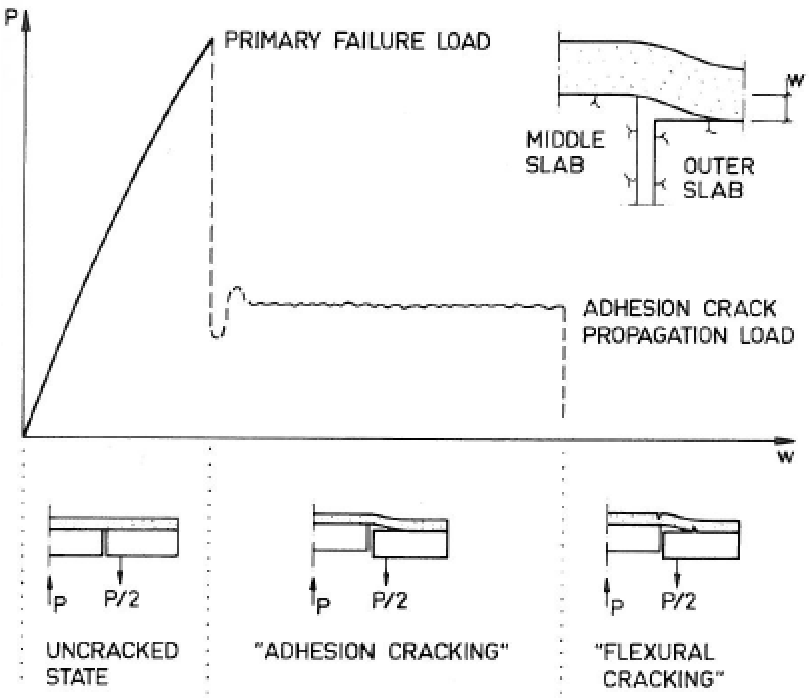

Figure 3.2 Failure modes with continued punch loading of a spray concrete layer (Holmgren 1979).

In order to estimate the capacity of a spray concrete lining to resist punching, a simplified load case can be assumed, Figure 3.3. As the most probable failure mode is adhesion cracking through punching, there is no need to calculate the bending moments. Adhesion cracking is independent of the layer thickness of the spray concrete in the range 20 to 80 mm.

The laboratory tests performed by Holmgren (1979) showed that load from adhesion cracking is distributed over a narrow band in the spray concrete (width = δ) approximately 0,003 m. In order to hold the block in place the stress induced on the contact surface, σ_{ad} should not exceed the adhesion crack resistance f_{ad}.

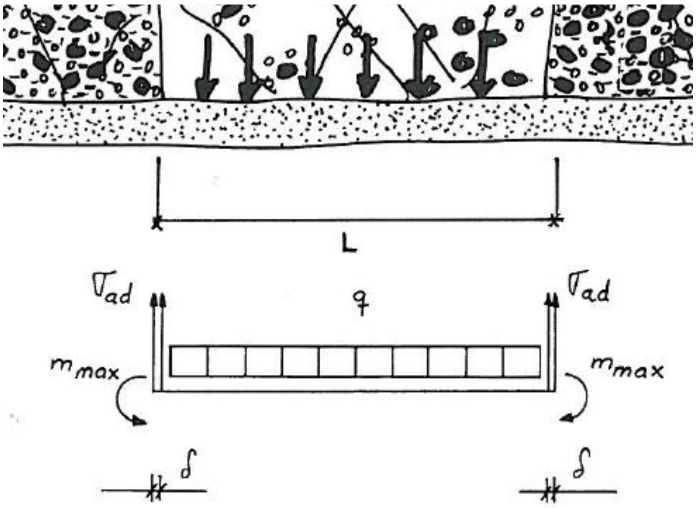

Figure 3.3 Adhesion cracking through punching, q is the load from a loose block in the tunnel roof, σ_{ad} is the stress on the bound between spray concrete and rock, L is the length of the block and δ is the width of the carrying stripe of the spray concrete (Holmgren 1992).

A vertical projection of the situation in Figure 3.3 gives:

$$qL - 2\sigma_{ad}\,\delta = 0 \qquad 3.1$$

From which

$$\sigma_{ad} = qL/2\delta \qquad 3.2$$

Where f_a is the strength of the bound between rock and spray concrete.

$\sigma_{ad} \leq f_a$ No failure 3.3

$\sigma_{ad} > f_a$ Tensile failure 3.4

Holmgren (1992) compiled earlier research on adhesion strength between the rock surface and the spray concrete. This includes studies by Barbo (1964), Karlsson (1980) and Hahn (1983).

The studies indicated that adhesion strength is depended on the rock type rather than the roughness of the rock surface. Surface coating from diesel exhausts reduced the adhesion strength proportional to the time of exposure during experiments, but the mechanisms still needs to be studied in detail. Flowing water has a strong negative influence on the adhesion strength and should be avoided. Typical values for f_a are presented in Table 3.1.

Table 3.1 After Hahn (1983) in Holmgren (1992).

Rock type	**Slate**	**Granite**	**Limestone**	**Sandstone**
f_a [MPa]	0,2-0,4	0,8 - 1,6	1 - 1,6	1,6 <

3.2.2 Spray concrete arcs

A punch loaded spray concrete arc will induce a normal stress parallel to the contact area between rock and spray concrete. If the arc is unsupported an adhesion crack can propagate along the arc. Figure 3.4 shows sketches of supported and unsupported spray concrete arcs. In order to take advantage of a spray concrete arc, it is important that the spray concrete is applied to and supported by the abutment or floor of the tunnel (Holmgren 1979).

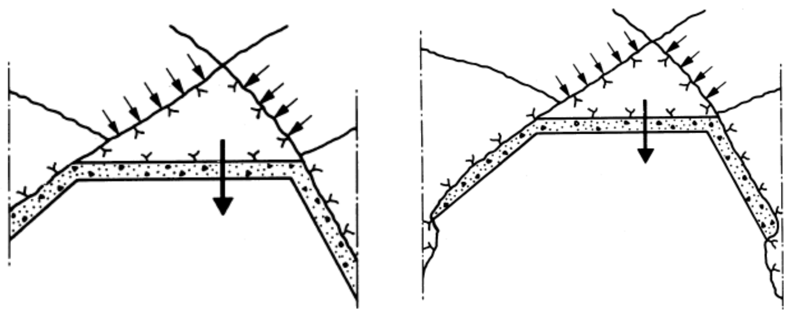

Figure 3.4 Sketches of supported and unsupported spray concrete arcs. Modified from Holmgren (1979).

3.2.3 Low-pH spray concrete in the repository

There are problems related to the use of conventional cementations material in the repository for spent nuclear fuel as alkalis are released into the leachates. These pulses are in the range of pH 12-13 and may disturb the function of the bentonite backfill. High pH may also increase alteration of fracture filling material and eventually contribute to solving of the spent nuclear fuel. In order to decrease the risk for those problems, leachates and pore-water from and in the concrete materials in the repository should have pH of 11 or lower.

During February 2004 to January 2009 a concept for low-pH sprayed concrete was developed within the ESDRED project (Engineering Studies and Demonstrations of Repository Design) were laboratory testing were conducted by Vattenfall AB in Älvkarleby, Sweden and by CBI and field tests were conducted in Äspö HRL. Based on the results additional tests were conducted in Äspö HRL, for example with steel fibre reinforcement (Bodén and Pettersson 2011).

3.3 Wire mesh

Different types of meshes are frequently used in underground construction in order to protect the personnel working underground from smaller block falls. The mesh is normally nailed to the rock surface with rock bolts and sometimes spray concrete can be applied over the meshes, which in this case will function as reinforcement. The normal material is steel but plastic wire meshes are also being used.

Bawden et al. (2000) describes wire mesh types and applications. Two types of steel wire mesh is commonly used, chain linked and wielded. Chain linked mesh is more ductile and easier to apply to a rough rock surface but if the surface is reasonable smooth and there is enough room to work a welded mesh is the better choice. Figure 3.5 shows chain linked and wielded wire mesh together with rock bolts who keep them in place.

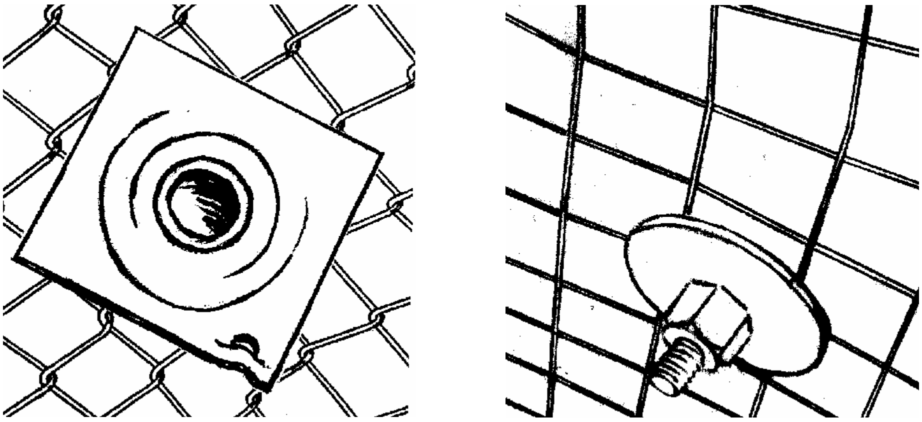

Figure 3.5 Chain linked wire mesh, left, and Welded wire mesh, right (Bawden et al. 2000).

Wire mesh has the advantage that the rock surface is assessable to inspection, mapping and other activities. It is also relatively easy to remove. A serious problem with wire mesh is corrosion. To avoid this mesh can, for example, either be galvanised or made of stainless steel.

3.3.1 Capacity of wire mesh

The capacity of a wire mesh depends on the material used, the diameter of the wires and the mesh aperture. In a simplified case a cubic block loading the mesh will force tension in the loaded steel wire. The capacity with equally loaded wires is:

$$F_{Mesh} = n\, \sigma_t \cdot A \qquad 3.5$$

Were F_{Mesh} is the total mesh capacity [MN], n is the number of loaded wires and σ_t [MPa] is the tensile strength of the material. A [m^2] is the area of the wire.

4 Experience from field work

This chapter summarizes the experience collected during the field work at Äspö HRL.

4.1 Mapping

4.1.1 Mapping of overbreak areas in the TASA access ramp

Mapping of overbreak areas in the tunnel roof of the TASA access ramp in Äspö HRL was conducted by the author. The results from this survey are presented in Ittner (2010). The work included mapping of the 3120 m TASA access tunnel, where causes for scaling and size of overbreak areas were mapped. In addition scaling records were used to calculate block mass distributions for each 20 m section of the access tunnel. Five different types of areas were mapped, Figure 4.1.

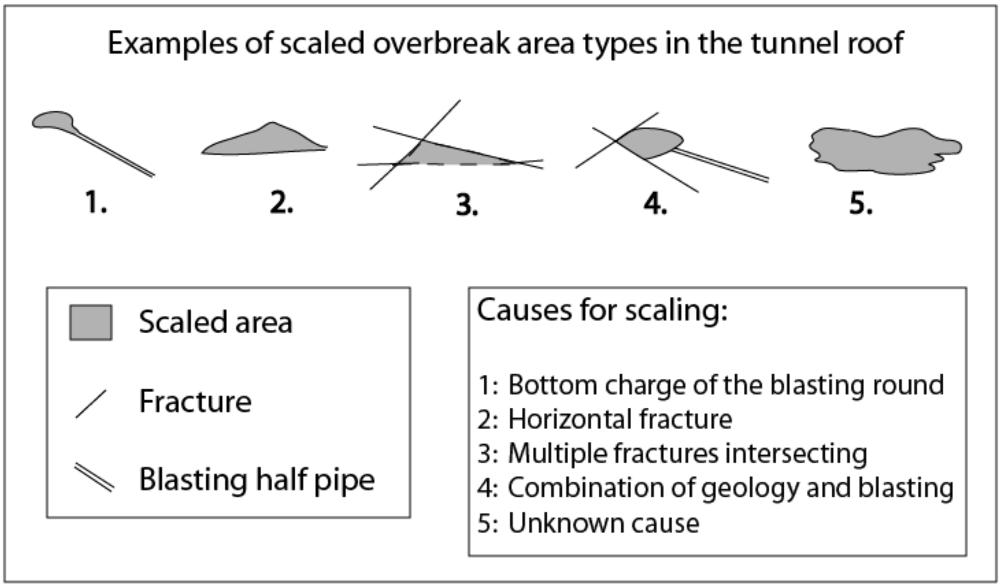

Figure 4.1 Different types of overbreak areas mapped in the TASA access ramp. Type 1 is located in the end of the blast rounds (Ittner 2010).

In addition to the mapping, a method was developed to evaluate the results from the mapping together with scaling records for the TASA access ramp. By distributing the scaled volumes over the mapped areas the mass of scaled blocks could be estimated for each scaling occasion, generalized to one scaling occasion each year, Figure 4.2.

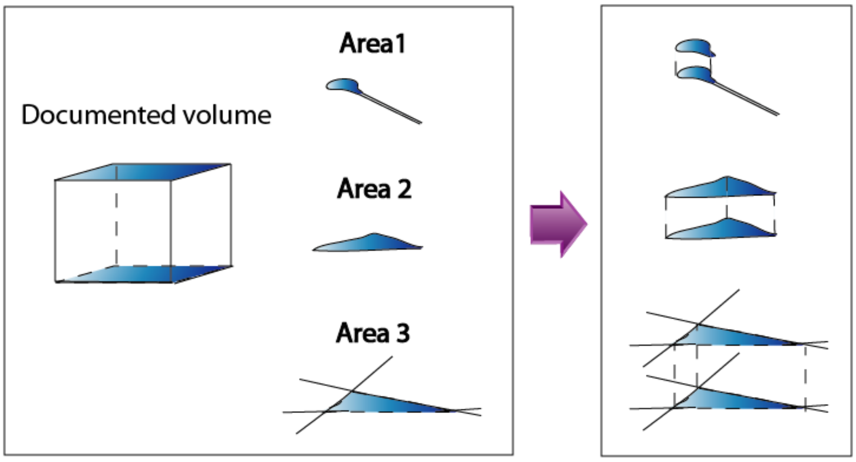

Figure 4.2 Method of evaluation of the scaling statistics modified after Ittner (2010).

One of the conclusions from this survey was that over 50% of the scaled overbreak areas were located in and caused by hole bottoms near the end of the blasting rounds. Those areas were generally small compared to the other types.

The high frequent scaling conducted in and near the ends of the blast rounds is a result of a combination of geometry and excavation damage. Due to the excavation method, where the contour holes are drilled with a certain look-out angle, the tunnel roof will achieve a *"saw tooth"* structure along the tunnel heading. Because of this the distance between drilling pipes is largest at the end of the blasting rounds. This is also where the bottom charge of the blasting rounds is located. Figure 4.3 shows the lognormal block mass distribution from the TASA access ramp with mean 182 kg and median 86 kg. This includes blocks of all the types in Figure 4.1. With assumed density of 2700 kg/m^3 the volume of the blocks could be 0,0674 m^3 and 0,0318 m^3.

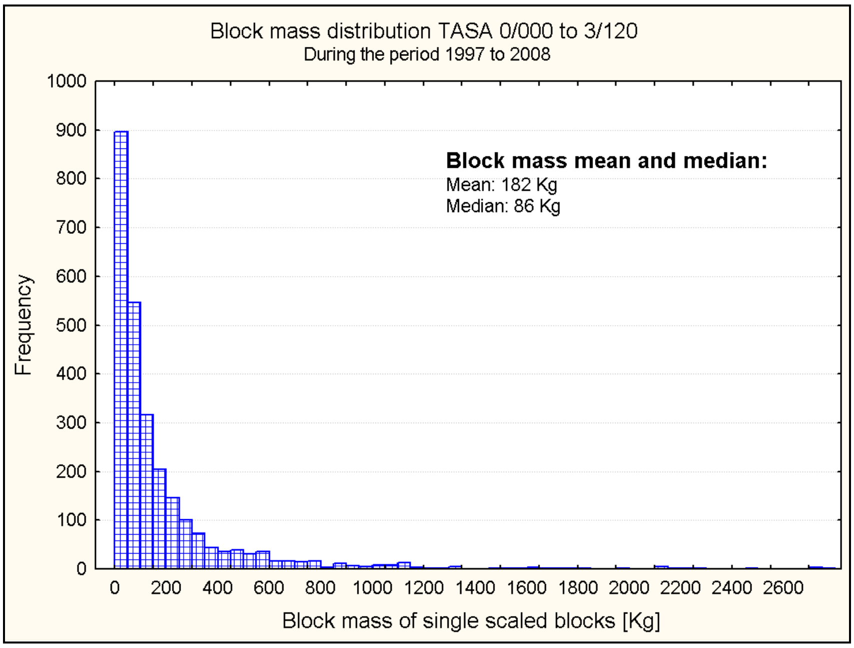

Figure 4.3 Lognormal block mass distribution from the TASA access ramp. The block mass distribution is back-calculated by (Ittner 2010) based on the method presented in Figure 4.2.

4.1.2 Inspection and mapping for reinforcement of blast round ends

In February 2011 an inspection of the TASS tunnel was conducted in order to obtain a basis for the support design. Several features were noted during the mapping:

- Avoiding geometry in the transition area between two blasting rounds.
- Intersecting fractures, forming wedges.
- Maintenance scaling in blast round ends.
- Maintenance scaling due to blast damage.
- Rock loosened by blast damage in otherwise undisturbed rock mass.

In addition to this mapping of scaled blocks with a combination of blast damage and geology were conducted.

The three possible solutions were spray concrete, wire mesh or continued maintenance scaling. In the three last rounds a backfill test will be conducted later on and wire mesh was selected as rock support in this part of the tunnel in order to test its behavior during backfill. Rock support was proposed for sections were problems could be expected. The information collected during the mapping, is presented by Söder (2011), see appendix E. Table 4.1 shows the results from the mapping: a rock support recommendation for each section. Note that the last three sections were suggested for a backfill test project and therefore spray concrete was not recommended. The last section was hard to access due to a water filled depression. It is also located close to the tunnel face.

Table 4.1 Results from the mapping conducted in February 2011. The suggested rock support for each of the section is noted with a color. Green for maintenance scaling, yellow for wire mesh and grey for spray concrete.

Section [m]	**24,7**	**28,8**	**32,8**	**37,3**	**42**	**45,6**	**48,5**	**52,6**	**56,6**	**60,4**	**64,4**	**68,7**	**73**	**77**	**80,5**
Results from mapping															

4.2 Construction works

4.2.1 Spray concrete

The works with selective spray concrete in the TASS tunnel was conducted 2011-04-28 to 2011-05-03. The aim was to fill out the overbreak areas, smoothen the contour and to create a spray concrete arc in the end of the most damaged blast rounds.

Four sections were to be constructed, two of them in two layers, two sections with thickness 50 mm and two with thickness 100 mm. The maximum thickness was to be applied in the blast round end and then a decreasing thickness, filling overbreak areas. The area was marked before the works started, Figure 4.4.

Figure 4.4 The area was marked before the works started.

50 and 100 mm markers were placed in the roof, before the works started, in order to ease the work for the operator and insure the desired thickness. The contractor BESAB used a spray concrete robot with one operator, one miner for assistance and one work supervisor. The spray concrete was wet mixed and transported to the work site from a local concrete factory. There were several production stops due to malfunction of the spray concrete robot. The active production time was 4,5 min/m.

Rebounded spray concrete were to be weighted. For this purpose a nonwoven fabric, covering the tunnel floor, was used, Figure 4.5. The fabric was weighted from a wheel loader with the instrument in Figure 4.5.

Figure 4.5 Left: Nonwoven fabric and Right: Weighting instrument.

The fabric together with rebounded spray concrete was weighted. The results were influenced by the malfunctions. The results are summarized in Table 4.2.

Table 4.2 Mass and volume of rebounded spray concrete.

Spray concrete section	**1** **(62 - 67 m)**	**2** **(53,5 - 60 m)**	**3+4** **(34,5 - 45,5 m)**
Rebound mass [kg]	-	222	1262

Despite the many problems with malfunctioning spray concrete equipment, the results are satisfactory, Figure 4.6.

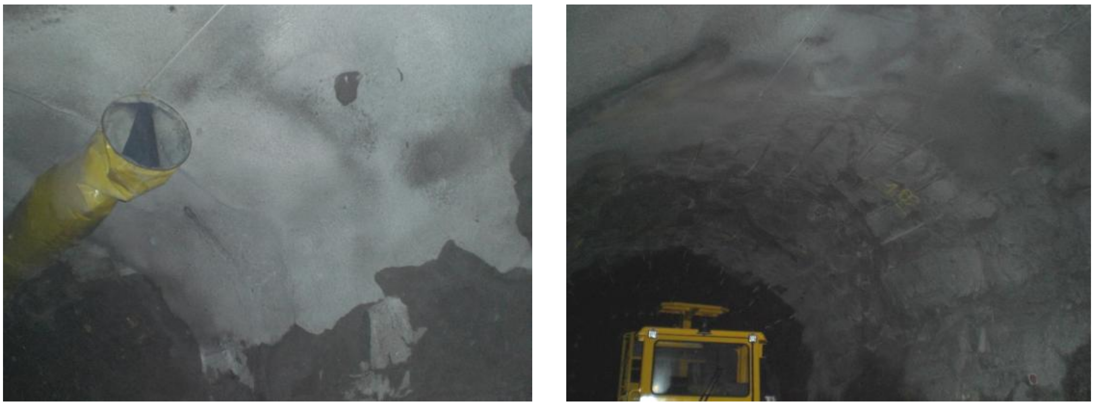

Figure 4.6 Results of the spray concrete works.

After the spray concrete works was finished a second laser scanning of the tunnel was preformed. By comparing the previous laser scanning with the new one, the volume, mass and rebound of applied spray concrete could be estimated for each section, Table 4.3.

Table 4.3 Spray concrete area, volume, mass and rebound for each section estimated by comparing the two conducted laser scannings. The mass was calculated from the volumes assuming a density of 2200 kg/m^3.

Section [m]	**Area [m^2]**	**Volume [m^3]**	**Mass [kg]**	**Rebound [%]**
34,5 - 45,5	38,68	1,32	2904	43
53,5 - 60	23,09	0,49	1078	20
62 - 67	18,85	0,52	1144	-

Figure 4.7 depicts the sections with applied spray concrete, based on the two laser scannings conducted.

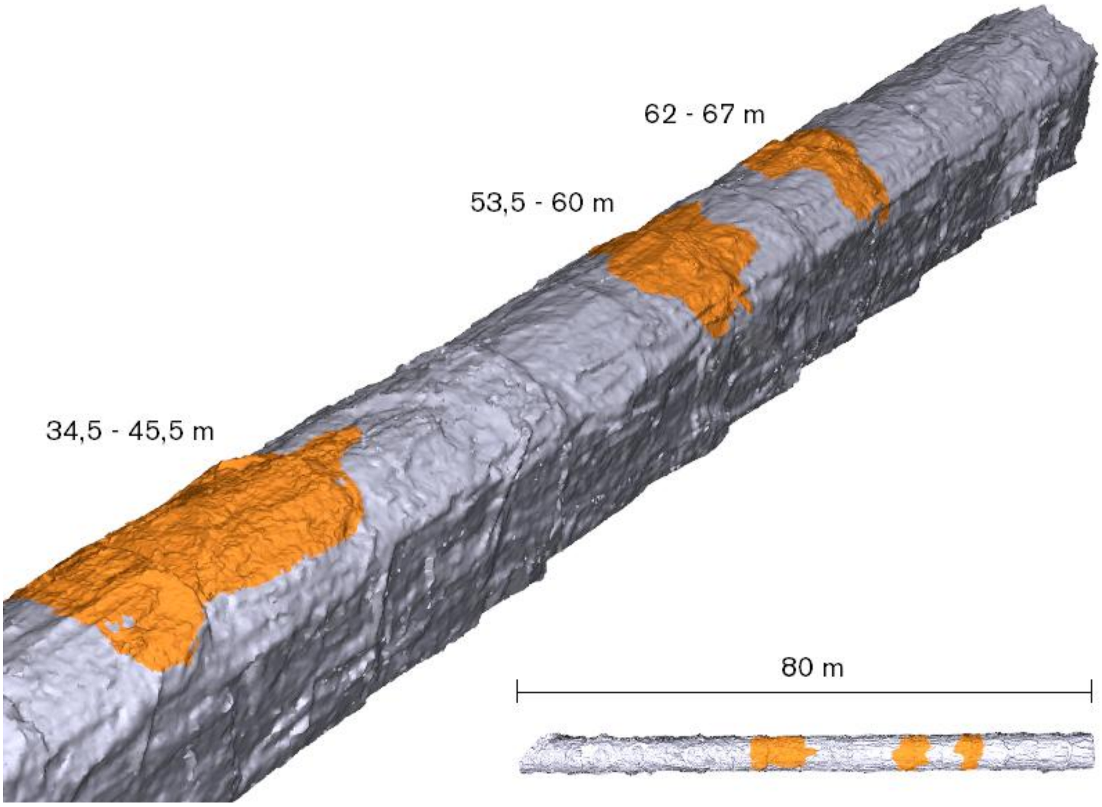

Figure 4.7 Sections with applied spray concrete, based on the two laser scannings. Spray concrete is marked orange in the figure. Figure by Pär Kinnbom (modified).

4.2.2 Mesh

Wire mesh was installed in four selective sections of the TASS tunnel during May 2011. Contractor for the project was Södermans bergssprängning AB. Gunnebo industrial fence was used together with 0,8 m grouted rock bolts. The bolt spacing was 0,8 m.

The installation of wire mesh was conducted by two miners in three stages:

1. Drilling of holes for the rock bolts

2. Grouting of the holes and installation of rock bolts. The production steps were:
   Mixing of grout, grouting of holes and installation of bolts. After finished production the workspace must be cleaned.

3. Installation of wire mesh. The production steps were: Measuring and cutting of mesh and installation of mesh.

The Figures 4.8 to 4.13 depicts different stages in the installation process.

Figure 4.8 Installed bolts in the roof.

Figure 4.9 Installation of mesh.

Figure 4.10 Applied mesh before tensioning.

Figure 4.11 Tensioning of rock bolts.

Figure 4.12 Applied mesh.

Figure 4.13 Applied mesh.

Each of the stages requires preparations before the activity can be carried out. Examples are mixing and testing of grout and measuring and cutting of wire mesh sections. Measured times for activities and preparations are presented in Appendix D. The mean production times for the production steps are presented in Table 4.4. The production time for the drilling includes preparations, transport etc. The production times for grouting and installation of wire mesh are active production times.

Table 4.4 Production times for wire mesh.

Activity	**Time/ m, mean values [h/m]**
Drilling	0,83
Grouting	0,03
Installation	0,08

5 Analysis

5.1 Stress modeling of excavation with uneven contour

A stress model of the TASS tunnel stress situation has been established using the finite element program Phase[2] released by Rock Ware (Manual download able from www.rockscience.com). The program uses boundary elements.

The purpose of the modeling was to evaluate how the contour of the excavation effects the distribution of induced stress.

5.1.1 Model setup and input data

From the laser scanning of the TASS tunnel conducted in 2009 cross sections has been cut out in 15 tunnel sections. The sections are located approximately 0,2 meter behind the measured section of the face in each round, i.e. in the area where most of the block falls and scaling could be expected.

The model was constructed using a graded mesh with 3-node triangular elements. Figure 5.1 shows the generated mesh in section 24,7 m. The stress field is assumed constant with in situ stresses σ_{h1}, σ_{h2} and σ_v. σ_{h1} and σ_v are the major and minor in plane principal stresses and σ_{h2} is the out of plane in situ stress. In the model, σ_{h1}, σ_{h2} and σ_v are defined as σ_1, σ_3 and σ_2, as σ_{h2} and σ_v both have the magnitude of 13 MPa.

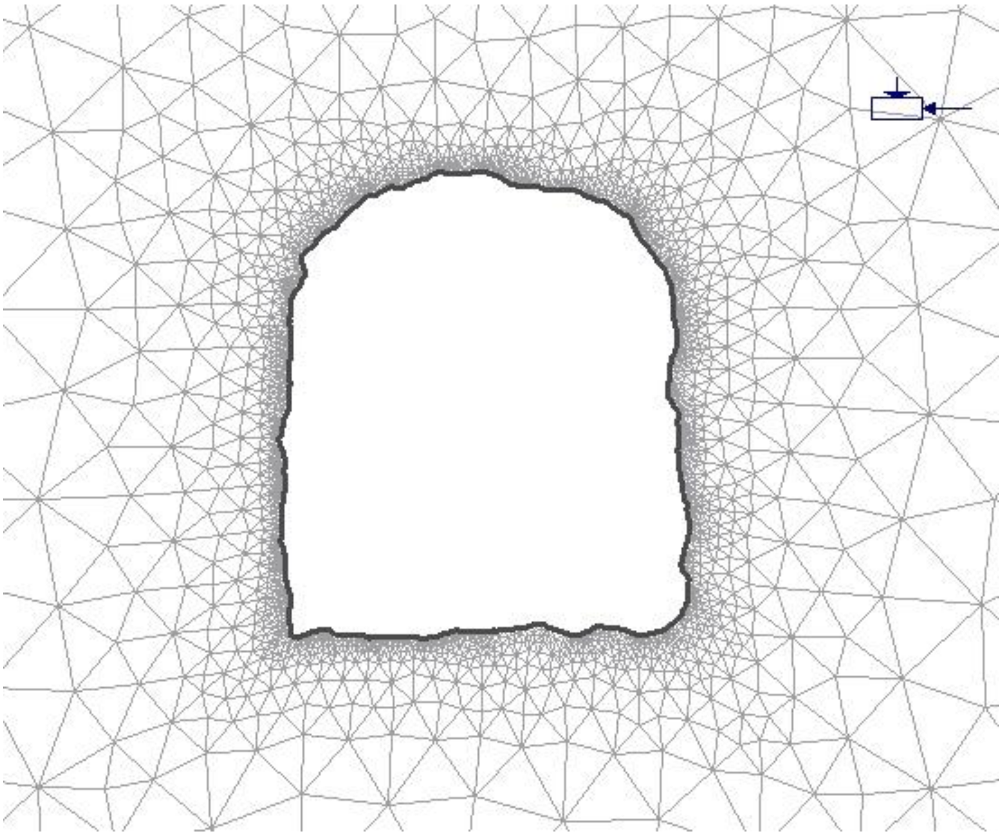

Figure 5.1 The mesh for the section 24,7 m, a graded mesh with 3-node triangular elements.

A 2D model was chosen due to the favorable in-situ stress situation in the bedrock, were σ_{h1} acts orthogonal to the tunnel heading. This minimizes shear stress in the rock mass which in turn reduces the need for a full 3D simulation.

The model is based on the Mohr-Colomb failure criteria and the rock mass is assumed to be elastic.

5.1.2 Stress simulation of excavation with theoretical profile

A simulation of the theoretical profile of the TASS tunnel was conducted, to be used as a reference to the simulations based on the laser scanned contour. Figure 5.2 depicts the distribution of induced principle stress σ_1, resulting from the in situ stress σh_1, 0,001 m in the rock mass from the excavation boundary.

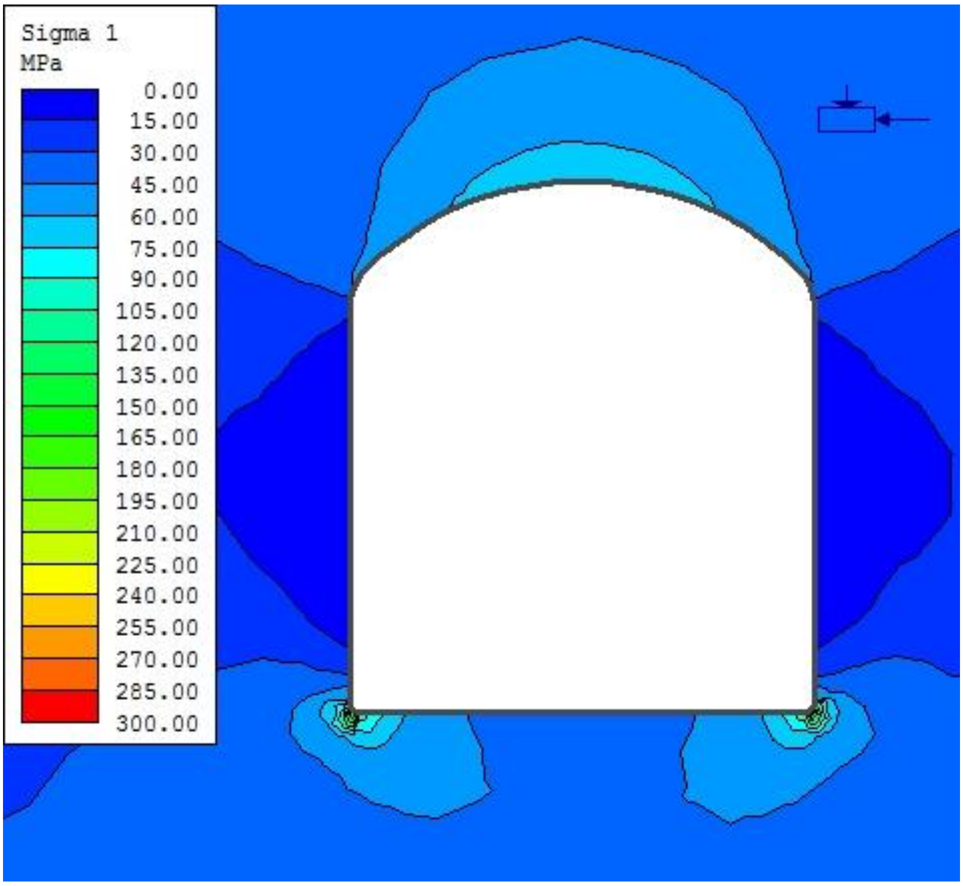

Figure 5.2 Stress field of the induced principal stress σ_1 for the theoretical profile. Note the relatively high stress magnitude in the roof and the lower stress magnitude in the tunnel walls.

The stress distribution in the tunnel roof of the theoretical profile is given in Figure 5.3 together with lines representing minimum values for crack initiation and spalling strength in the rock. Figure 5.4 shows the distribution of σ_3 for the theoretical section.

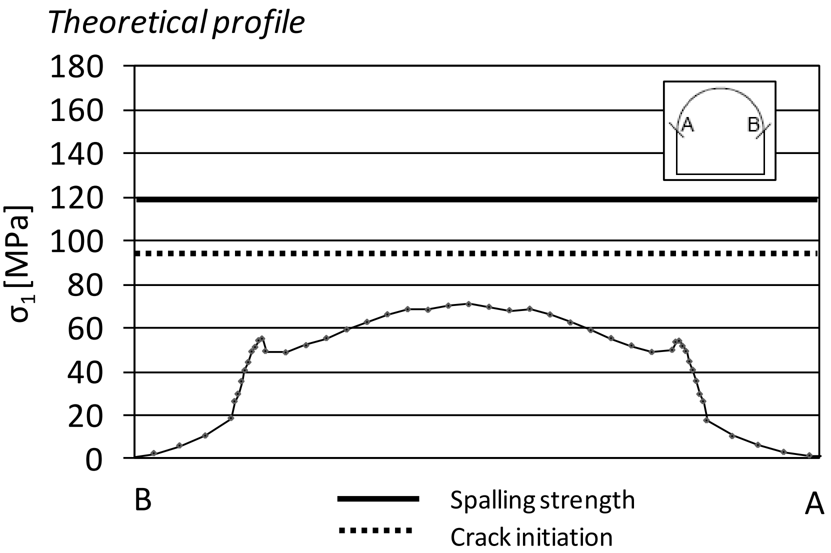

Figure 5.3 Stress distribution (σ_1) in the tunnel roof of the theoretical profile. Limits for crack initiation and spalling strength are noted in the figure. Notice the smooth curve and the distance to the crack initiation and spalling limits.

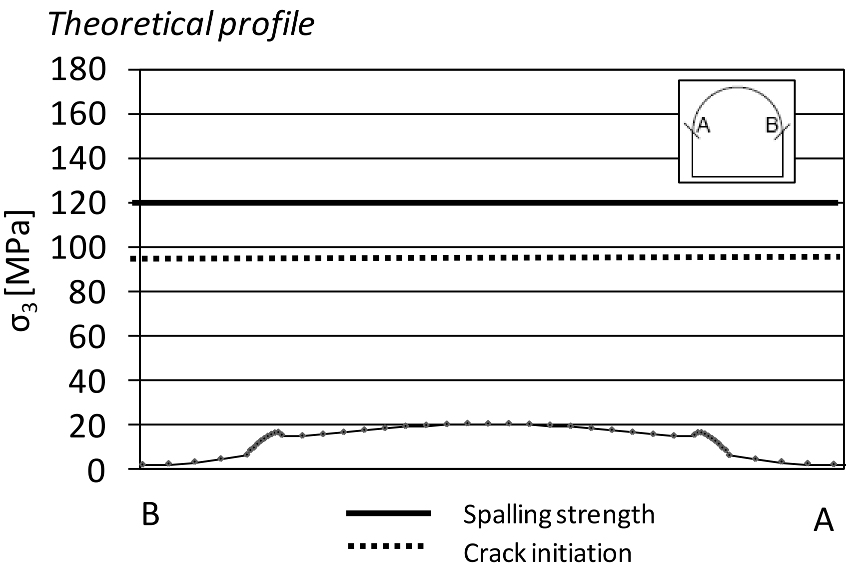

Figure 5.4 Stress distribution (σ_3) in the tunnel roof of the theoretical profile. Limits for crack initiation and spalling strength are noted in the figure. Notice the smooth curve and the distance to the crack initiation and spalling limits.

5.2 Stress simulation of excavation with uneven contour

Presented underneath are the distributions of induced principle stress 0,001 m in the rock mass from the excavation boundary for one example section. Results from additional sections are found in appendix B. Figure 5.5 shows the stress field of the induced principal stress σ_1 in section 24,7 m.

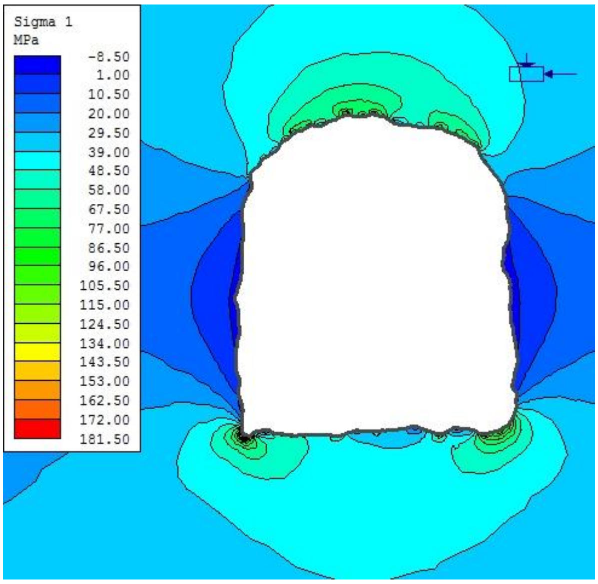

Figure 5.5 Stress field of the induced principal stress σ_1 in section 24,7 m. Observe the concentrations of high and low stress peaks in the tunnel roof.

Figure 5.6 shows the distribution of induced principle stress in the roof of the same section. Crack initiation and spalling strength limits are noted in the figure.

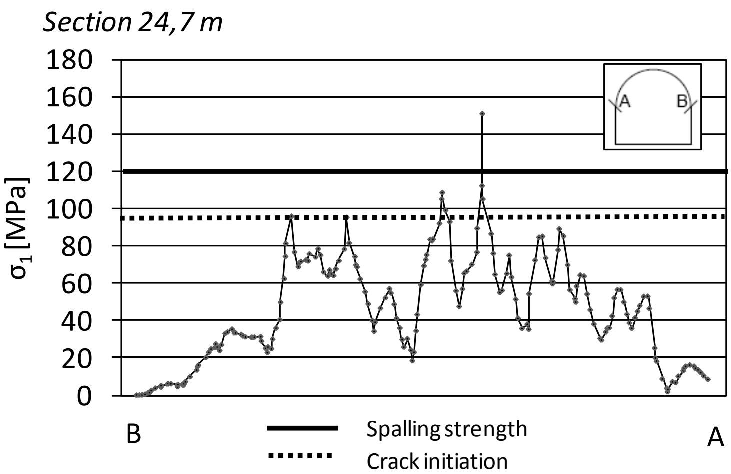

Figure 5.6 Stress distribution (σ_1) in the tunnel roof of the section 24,7 m. Observe that several stress peaks exceeds the crack initiation and spalling limits. The distribution is presented in the opposite heading in relation to Figure 5.5, i.e. the tunnel is displayed heading in the opposite direction.

The stress magnitudes in section 24,7 m of the minor induced principle stress σ_3 is presented in Figure 5.7. The stress distribution in the tunnel roof is presented in Figure 5.8. The heading is orthogonal to σ_1 and out of the plane.

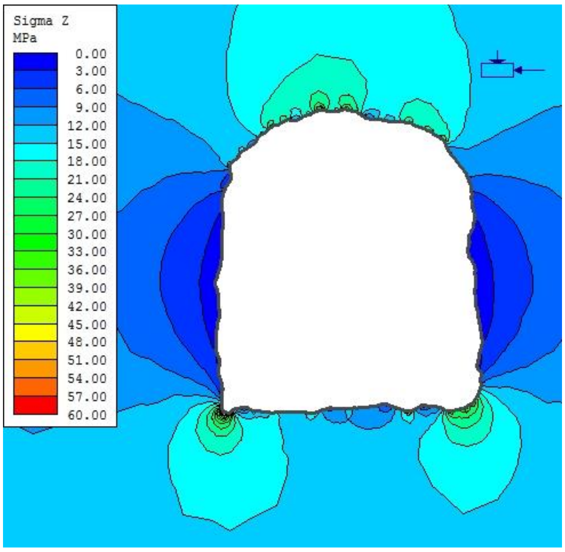

Figure 5.7 Stress field of the induced principal stress σ_3 in section 24,7 m. σ_3 is orthogonal to σ_1 and results in the same locations of stress peaks but the magnitude is lower.

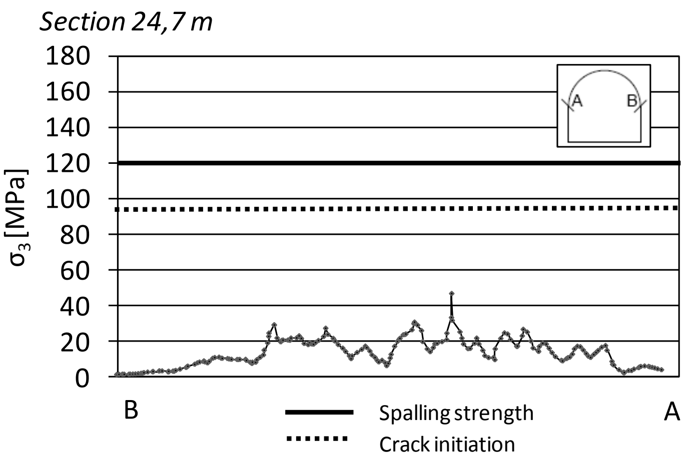

Figure 5.8 Stress distribution (σ_3) in the tunnel roof of the section 24,7 m. Observe the lower magnitudes compared to σ_1. The distribution is presented in the opposite heading in relation to Figure 5.7, i.e. the tunnel is displayed heading in the opposite direction.

The results suggests that a uneven surface leads to a uneven stress distribution in the rock mass, with several extreme points of high and low stress. This can give an idea of the failure modes in the different sections. High stress increasing the risk for spalling and low stress increases the risk for other types of block falls, resulting from relaxation.

5.3 Cost analysis

This chapter analyses how the construction costs differ between different support alternatives. During the field work active production times for the different work steps were measured. Costs for machinery, personnel and material were acquired through personal communication with the contractors during the field work. The collected material is found in appendix D.

The calculation does not consider costs of work site establishment as the focus is a large scale production in the deposition area of the planned repository for spent nuclear fuel. The aim of this calculation is not to estimate the total cost of each individual alternative but to calculate the costs with the same approach in order to compare them to each other.

Based on the observations during field work the following costs for the spray concrete works pro square meter could be identified, Table 5.1.

Table 5.1 Costs pro square meter spray concrete.

Type of cost	**Activity**	**Cost [SEK/m^2]**
Machinery	Spray concrete robot/ m^2	15,05
Personnel	Two miners	11,90
	Work supervisor	6,40
Materials	Spray concrete /m^2	91,42
	Additive 2,5 % of volume	2,74
	Parts 10% of costs	9,14
Total cost/m^2		136,66

The cost calculation for the wire mesh works are presented in table 5.2.

Table 5.2 Costs pro square meter wire mesh.

Type of cost	Activity	Cost [SEK/m^2]
Machinery	Drill rig	65,11
	Platform	4,66
Material	Cement	14,69
	Bolts	286,8
	Wire mesh	102,5
Personnel	Drilling	145,83
Two miners	Grouting	4,86
	Installation	13,77
Total cost/m^2		638,22

The result pro meter suggests that the production cost pro m^2 of spray concrete is approximately 20 % of the cost for wire mesh. This is however based on active production times. The actual production times include moving of the work platform or spray concrete robot and cleaning of workspace etc. Including those parts of the total production time would increase the costs for wire mesh more rapidly as more time consuming work steps are needed. For the spray concrete works the costs for spray concrete is most dominating and there are reasons to believe that prices could be lower in a large scale project. This supports the estimation that the spray concrete is more cost effective then wire mesh.

5.4 Reinforcement capacity

Presented in this chapter are calculated capacities of spray concrete and wire mesh to carry expected loads.

5.4.1 Expected loads

The block mass distribution of the TASA access tunnel could be used to estimate the mass of a theoretical loose block, loading the spray concrete or wire mesh reinforcement in the TASS tunnel. The purpose of the lining is not to reinforce larger blocks or wedges of the area types 2 and 3. Those blocks will require selective spot bolting. In addition the blocks of type 1 and 4 are relatively small and frequent in the area were support is relevant. Based on the lognormal structure of the block mass distribution the mean value represents a value that is significantly large and *on the safe side* if used as a basis for calculations. When the good quality of the blasting works in the TASS tunnel is considered, the median value is probably more in the range of an expected load. For the calculations cubic block forms are assumed, see Table 5.3.

Table 5.3 Possible block sizes.

Block	Mass [kg]	Length of side [m]
Median	182	0,422
Mean	86	0,509

5.4.2 Capacity of spray concrete

Based on the formulas in chapter 3 the capacity of spray concrete was evaluated. The calculated factors of safety are found in Table 5.4.

Table 5.4 Evaluated factors of safety for the spray concrete.

Block	Required f_a [MPa]	FS for $f_a = 0,8$ [MPa]	FS for $f_a = 1,5$ [MPa]
Median	0,33	2,4	4,5
Mean	0,58	1,4	2,6

5.4.3 Capacity of wire mesh

The capacity of welded and chain linked wire mesh has been evaluated, based on the method in chapter 3. The chain linked industrial fence manufactured by Gunnebo and the welded Ripinox by the Swiss manufacturer ANKABA was used as examples. The properties are found in the product description for the two mesh types (Gunnebo *Gunnebo industristängsel Kvalitet över tiden*) and for the welded wire mesh (ANKABA (2008) *RIPINOX® Edelstähle und Stahlmatten für Stahlbetonbau Aciers inox et treillis soudés pour constructions en béton armé).* The calculated factors of safety are found in Table 5.5 and Table 5.6.

Table 5.5 Evaluated factors of safety for the chain linked wire mesh from the Swedish manufacture Gunnebo AB.

Block	Mesh capacity [kN]	Load on mesh [kN]	FS
Median	53,69	0,84	64
Mean	64,76	1,78	36

Table 5.6 Evaluated factors of safety for the welded wire mesh ripinox from the swiss manufactor ANKABA.

Block	**Mesh capacity [kN]**	**Load on mesh [kN]**	**FS**
Median	159,70	0,84	157
Mean	132,40	1,78	90

6 Method of evaluation

In order to analyze the need for reinforcement a multi criteria analysis was preformed. The analysis includes the parameters from evaluation of available statistics, mapping and simulations.

6.1 Rock mechanical model and failure mechanisms

Based on the mapping preformed in the TASA access ramp and the TASS tunnel and the simulations conducted three main types of failure modes could be identified:

1. Cracking or spalling induced by high induced principle stresses around the excavation.

2. Gravity driven falls of block or wedges resulting from intersecting fractures and low stresses or tension.

3. Loose blocks resulting from blast damage due to geological fractures. These blocks can currently be stable but can risk falling due to stress variations initiated by for example heat producing machinery or other activities in the tunnel.

The primary failure modes related to the case of study are the types 1 and 4. Block falls of the type number 2 will most likely require individual bolting. In addition low stress or tension was most frequently located in the tunnel walls. This aspect reduces the need for including low stress in the analysis and therefore only σ_1 is considered in the multi criteria analysis.

A rough contour leads to concentrations of low and high stress. If the induced principle stress exceeds the crack initiation limit, the risk for cracking and spalling is increased. If however there are indications tension in a section a loose block is no longer locked by the induced principle stress.

The presence of geological fractures is a condition for the structural failure types to occur. High density of fractures increases the risk for blast damage.

6.2 Classification of end sections of blast rounds

The maintenance strategy for the TASS tunnel includes maintenance scaling, wire mesh and spray concrete. All of these maintenance strategies have different advantages and disadvantages. Support can be applied in sections where there is a risk for rock falls based on indications of damage in the rock mass. The level of damage indication can be determined from the results of mapping, statistics and simulation of the stress situation.

Through evaluation of the sections in the TASS tunnel the following matrix can be used to quantify and determine the damage indication level of each feature in a section. The total impression of a section can then be used to determine the type of rock support. Table 6.1 shows the numbers features that determine the damage indication level in a section.

Table 6.1 Number of features that determines the damage indication level.

Damage indication level	fractures	$\sigma_1 \leq 0$	$\sigma_1 > \sigma_{Crack}$	$\sigma_1 > \sigma_{spalling}$
Low	0-5	0-1	0-2	0
Medium	6-10	2	3	1
High	10<	3<	4<	2<

In sections with few extreme values in the stress field and low density of geological fractures there is no need for rock reinforcement and problems that could occur could be handled with maintenance scaling. Sections with low stress and a medium to high density of fractures could be reinforced with either wire mesh or spray concrete. Uneven surfaces, resulting in an extreme stress values are most efficient reinforced with spray concrete as the contact with the rock is better than with a wire mesh. As the fall outs in sections with high stress concentration, based on mapping experience, are small in size there is a possibility that they could fall through the gaps in the mesh.

The support alternatives can be chosen based on the damage indication level, presented in Table 6.1, and the magnitude of induced stress around the excavation. In order to assign reinforcement classes to the end sections of the blast rounds in a deposition tunnel, relevant parameters can be structured in a matrix, see Table 6.2. The matrix includes parameters from available statistics, mapping and simulations. In the cases were two alternatives are noted, the most cost effective one should be chosen, based on the cost analysis.

Table 6.2 Rock support for different magnitudes of damage indication level and type of feature. The support types are noted MS, WM and SC for maintenance scaling, wire mesh and spray concrete. For some combinations of parameters spray concrete or wire mesh can be used, depending on the production costs.

Damage indication level	Fractures	$\sigma_1 \leq 0$	$0 < \sigma_1 < \sigma_{Crack}$	$\sigma_1 > \sigma_{Crack}$	$\sigma_1 > \sigma_{spalling}$
Low	MS	MS	MS	MS	WM-SC
Medium	WM-SC	WM-SC	MS	WM-SC	SC
High	WM-SC	WM-SC	WM-SC	SC	SC

6.3 Recommendations based on results for each section

The recommendations based on the evaluation method in the chapter 6.2 are presented in Table 6.3.

Table 6.3 The method applied on the TASS tunnel. The damage indication levels low, medium and high are indicated with the colors green, yellow and red.

Section [m]	**Fractures [no]**	**$\sigma_1 \leq 0$ [No]**	**$\sigma_1 > \sigma_{Crack}$**	**$\sigma_1 > \sigma_{spalling}$**	**Recommendation**
24,7	8	0	2	1	Mesh/spray concrete
28,8	13	3	3	1	Mesh/spray concrete
32,8	12	3	5	0	Spray concrete
37,3	12	0	5	1	Spray concrete
42	5	1	4	3	Spray concrete
45,6	8	1	3	2	Spray concrete
48,5	8	0	2	1	Maintenance scaling
52,6	4	0	2	2	Mesh/spray concrete
56,6	7	0	2	1	Maintenance scaling
60,4	4	1	3	1	Maintenance scaling
64,4	13	1	5	1	Spray concrete
68,7	8	2	5	2	Spray concrete
73	4	1	2	2	Mesh/spray concrete
77	6	3	5	0	Spray concrete
80,5	7	3	1	1	Mesh/spray concrete

7 Discussion and conclusion

Compared to the theoretical section, with no stress peak exceeding the crack initiation limit, it is interesting to observe that all the evaluated sections from the laser scanning contains stress peeks in the tunnel roof, exceeding the crack initiation limit. There should however be no risk for large scale spalling or crack initiation as the curves generally are lower than the crack and spalling initiation limits. Stress induced block falls can therefore be considered to be limited in size.

The results of the production of the spray concrete are satisfactory. It was possible to smoothen the contour and to fill the overbreak areas. It was also possible to gradually decrease the thickness of the layer. Based on the literature survey, the layers should however not be thinner than 20 mm. It might be possible to create an arching effect in the spray concrete in the filled overbreak areas if the spray concrete can be supported by the edges of the area.

The results from the production of wire mesh are also satisfactory. The applied mesh, Gunnebo industrial fence, was easy to apply and has a good contact to the rock. As the mesh is single braided, the yielding of one single wire may cause a damage to propagate, leaving a large hole in the mesh.

Both spray concrete and wire mesh delivers acceptable factors of safety for the possible block loads. The difference in the factors depends on the fact that the loss of adhesion is compared to actual yielding of several wires. The loads are however *on the safe side*, which in turn would increase the actual factor of safety. For a single braided wire mesh, like Gunnebo industrial fence, the factor of safety may however be lower than the calculated values in chapter 6.4.3 due to the possibility of a propagating damage discussed earlier. Larger blocks should be spot bolted.

The contact between rock support and rock is far better if spray concrete is used. This affects the ability of the support to stabilize small stress induced outfalls.

Depending on the many time consuming work steps, the production of wire mesh have higher production costs compared to spray concrete. Therefore it is questionable to use wire mesh, as it does not have any technical advantage over spray concrete.

Table 7.1 presents the recommended rock support for the end of blast rounds in the TASS tunnel based on two methods, theoretical evaluation and mapping. In addition a recommendation based on the theoretical evaluation with construction costs considered are included.

There is a clear trend of coincidence between the recommendation based on the mapping and the recommendation based on the theoretical evaluation, especially considering that the last three sections was suggested for a backfill test project and therefore spray concrete was not recommended based on the mapping. The theoretical evaluation captures the overall trend for the tunnel with a need for rock support from approximately 25 m to 45 m and from 65 to 80 m. The sections between 45 and 65 can be handled with maintenance scaling.

Table 7.1 Recommendations from the mapping, the theoretical evaluation and the theoretical evaluation with construction costs considered. The suggested rock support for each of the section is noted with a color, green for maintenance scaling, yellow for wire mesh and grey for spray concrete. In the theoretical evaluation yellow suggests the use of either wire mesh or spray concrete, as both support alternatives could handle the expected problems.

Section [m]	24,7	28,8	32,8	37,3	42	45,6	48,5	52,6	56,6	60,4	64,4	68,7	73	77	80,5
Mapping															
Theoretical evaluation															
Theoretical evaluation (with construction costs considered)															

The Reinforcement of deposition tunnels in the repository for spent nuclear fuel should focus on the areas with the most documented problems, i.e. the sections in the ends of the blast rounds. Support for those sections should be considered based on deviations in geometry and density of geological fractures. Further development of the method should consider maintenance scaling statistics, however this requires good documentation.

The recommended rock support alternative, based on the experience from the TASS tunnel, is spray concrete as it gives a better result with less use of recourses. A more effective method of wire mesh installation may make the alternative competitive with spray concrete. Further field studies should, in addition to develop the method of wire mesh installation, include other types of wire mesh. Welded wire mesh or wire mesh with a more complex braiding or twisting should be a safer rock support then a single braded wire mesh.

8 References

AB Svensk byggtjänst. (1998): *Anläggnings AMA 98. Allmän material- och arbetsbeskrivning för anläggningsarbeten.* Chapter CBC: Bergsschakt, pp 41-51.

Andersson C. Malmtorp J. (2009): *Berguttag i TASS tunneln. Delresultat t o m September 2008*. Svensk kärnbränslehantering AB, Report R-08-122, Stockholm, Sweden, 133 pp.

Andersson C. Söderhäll J. (2001): *Rock mechanical conditions. A study of correlation between geology, tunnel maintenance and tunnel shape.* Svensk Kärnbränslehantering AB. Report R-01-53, Stockholm, Sweden, 64 pp.

Andersson J.C. (2007): *Äspö Hard Rock Laboratory. Äspö Pillar Stability Experiment, Final report. Rock mass response to coupled mechanical thermal loading.* Svensk Kärnbränslehantering AB, Technical Report TR-07-01, Stockholm, Sweden, 221 pp.

Andersson J.C. Staub I. (2004): *Äspö Pillar Stability Experiment Geology and mechanical properties of the rock in TASQ*. Svensk Kärnbränslehantering AB, Report R-04-01, Stockholm, Sweden, 210 pp.

Bawden W.F. Hoek E. Kaiser P.K (2000)**:** *Support of underground excavations in hard rock.* Downloaded 6 May 2011 from http://www.rockscience.com/education/hoeks_corner

Berglund J, Curtis P, Eliasson T, Olsson T, Starzec P, Tullborg E. (2003): *Äspö Hard Rock Laboratory. Update of the geological model 2002.* Svensk Kärnbränslehantering AB, Internal Progress Report IPR-03-34, Stockholm, Sweden, 130 pp.

Bodén A. Pettersson S. (2011): Unpublished manuscript to a Report. Svensk Kärnbränslehantering AB, Report R-11-XX, Stockholm, Sweden.

Eriksson M. Petersson J. Leander M. (2009): *Underground design Laxemar Layout D2.* Svensk Kärnbränslehantering AB, Report R-09-10, Stockholm, Sweden, pp 58.

Fredriksson A. Janson T. Staub I. (2003): *Äspö Hard Rock Laboratory Äspö Pillar Stability Experiment Geology and properties of the rock mass around the experiment volume.* Svensk Kärnbränslehantering AB, Internal Progress Report IPR-03-02, Stockholm, Sweden, 119 pp.

Hardenby C.J. Sigurdsson O. (2010): *Äspö HRL. The TASS-tunnel. Geological mapping.* Svensk Kärnbränslehantering AB, Report R-10-35, Stockholm, Sweden, 253 pp.

Hoek E. (2007)**:** *Practical Rock Engineering.* Downloaded 19 June 2011 from http://www.rockscience.com/education/hoeks_corner

Holmgren J. (1979): *Punsch-loaded shotcrete linings on hard rock*. Royal Institute of Technology, No. 121:6, Stockholm, Sweden.

Holmgren J. (1992): *Bergförstärkning med sprutbetong.* Vattenfall Vattenkraft, Vällingby, Sweden, 74 pp.

Ittner H. (2010): *Äspö Hard Rock Laboratory. Evaluation of scaling records for TASA access tunnel.* Svensk Kärnbränslehantering AB. Internal Progress Report IPR-10-01, Stockholm, Sweden, 28 pp.

Jansson T. Stigsson M. (2002): *Test with different stress measurement methods in two orthogonal bore holes in Äspö HRL*. Svensk Kärnbränslehantering AB, Report R-02-26, Stockholm, Sweden, 173 pp.

Johansson E. Karlzén R. (2010): *Slutrapport från drivningen av TASS-tunneln.* Svensk Kärnbränslehantering AB, Report R-10-31, Stockholm, Sweden, 210 pp.

Kirsch, G. (1898): Die Theorie der Elastizität und die Bedürfnisse der Festigkeitslehre. *Zeitschrift des Vereines deutscher Ingenieure*, Vol. 42, 1898, pp 797-807.

Lindblom U. (2010): *Bergbyggnad.* Liber, Stockholm, 240 pp.

Ljunggren C. Chang Y. Janson T., Christiansson R. (2003): An overview of rock stress measurement methods. *International Journal of Rock Mechanics and Mining sciences*: Vol. 40, pp. 975-989.

Martin D. (2009): *Decision bases for estimating the underground roof support required for operating a final repository*. SKBdoc ID 1266127, pp 6.

Söder P-E. (2011): *TASS tunneln Bergförstärkningar Rev A, 2011-03-25.* Vattenfall Power Consultant AB, Report, 10 pp.

World Stress Map Scandinavia. (2008): Heidelberg Academy of Science and Humanitas. Geophysical Institute University of Karlsruhe. Downloaded 28 May 2011 from http://dc-app3-14.gfz-potsdam.de/pub/stress_data/stress_data_frame.html

Contents - Appendices

A Geological map walls and roof

Legend

Scale: squares of grids on the maps 1x1 m

Green lines: fractures

Blue lines: water bearing fractures

Dashed lines: rock contacts

For more detailed description see Hardenby and Sigurdsson 2010.

Scanlines

Scanline mapping has been conducted in the end of the blasting rounds 6 to 20. The scan lines were placed 0, 2 meter behind the rounded value of the start section of the next round. The location of the scanlines is noted in the maps with black lines.

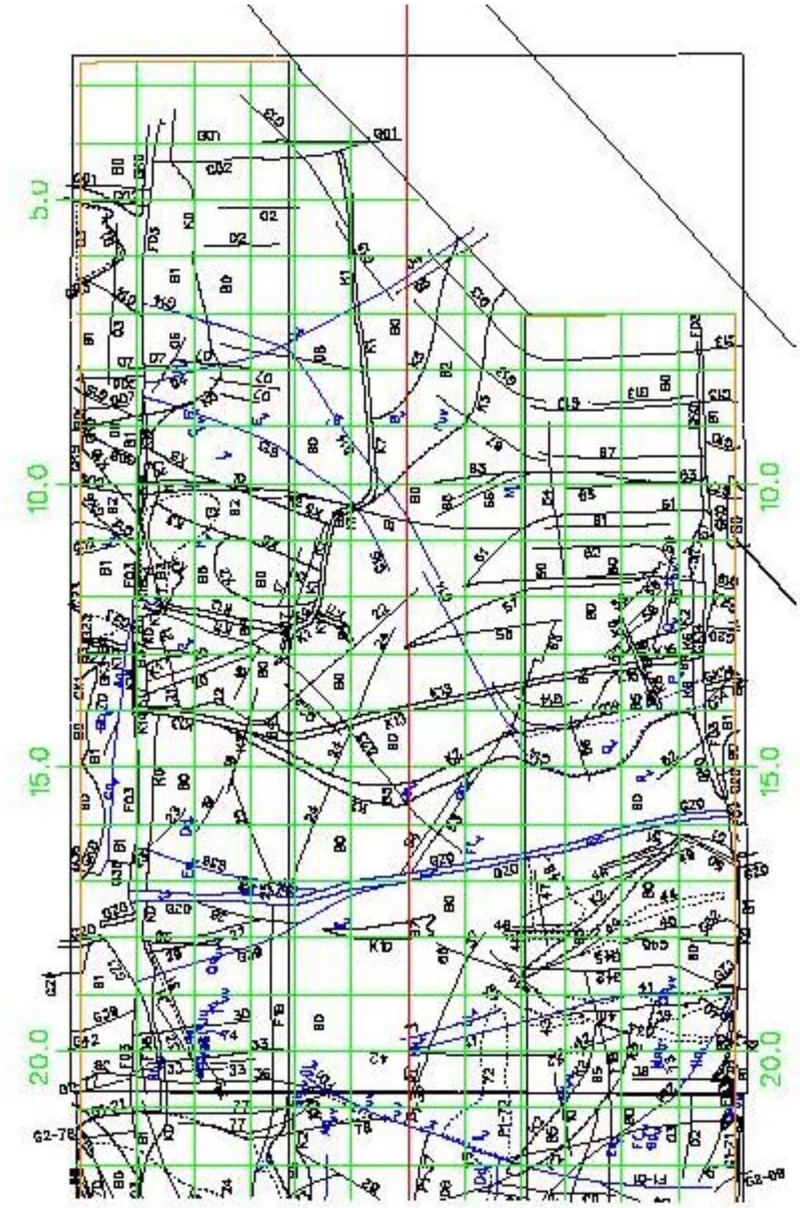

Figure A1: Geological map walls and roof section 0 to 22 m. Modified from Hardenby and Sigurdsson (2010).

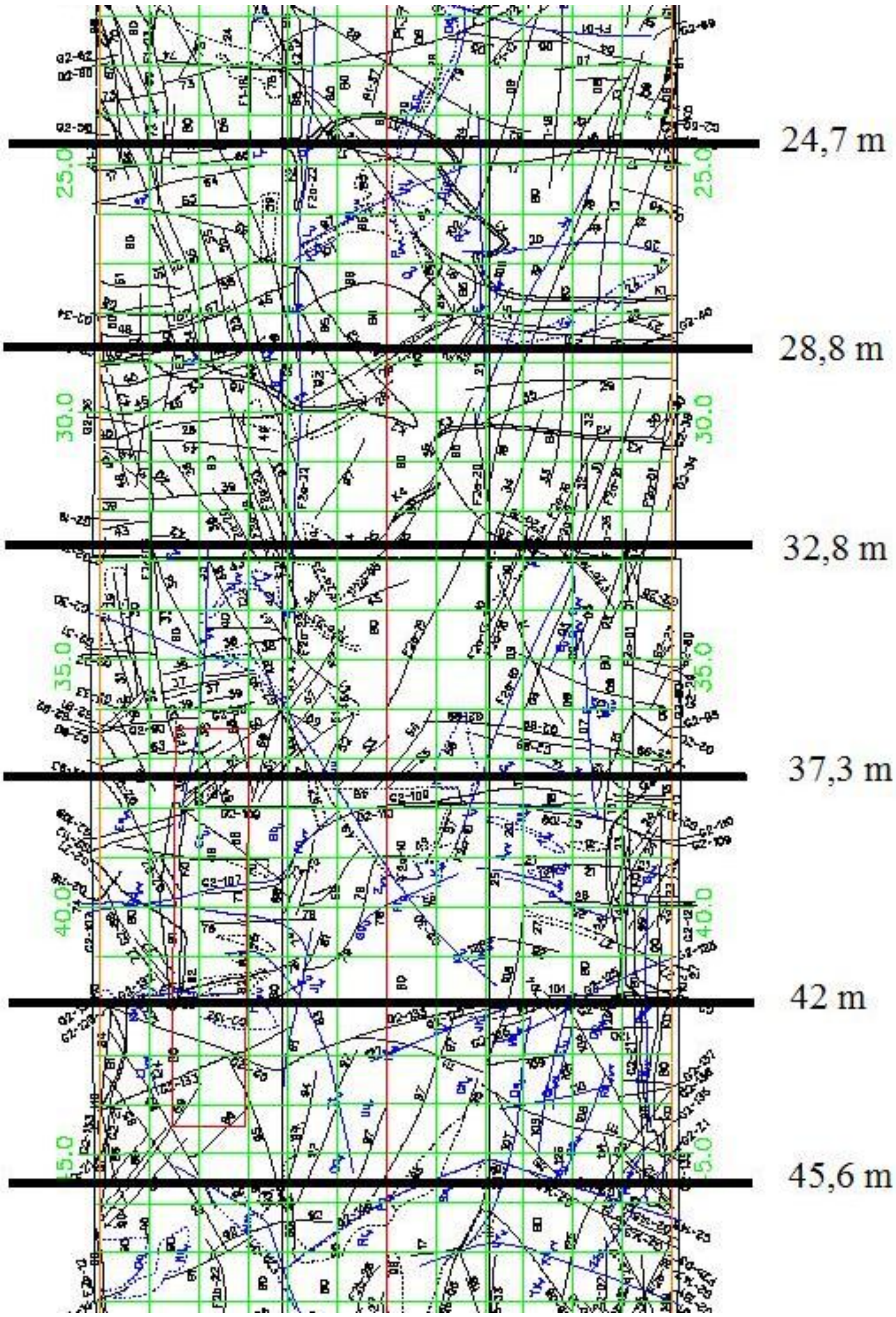

Figure A2: Geological map walls and roof section 22 to 48 m. Modified from Hardenby and Sigurdsson (2010).

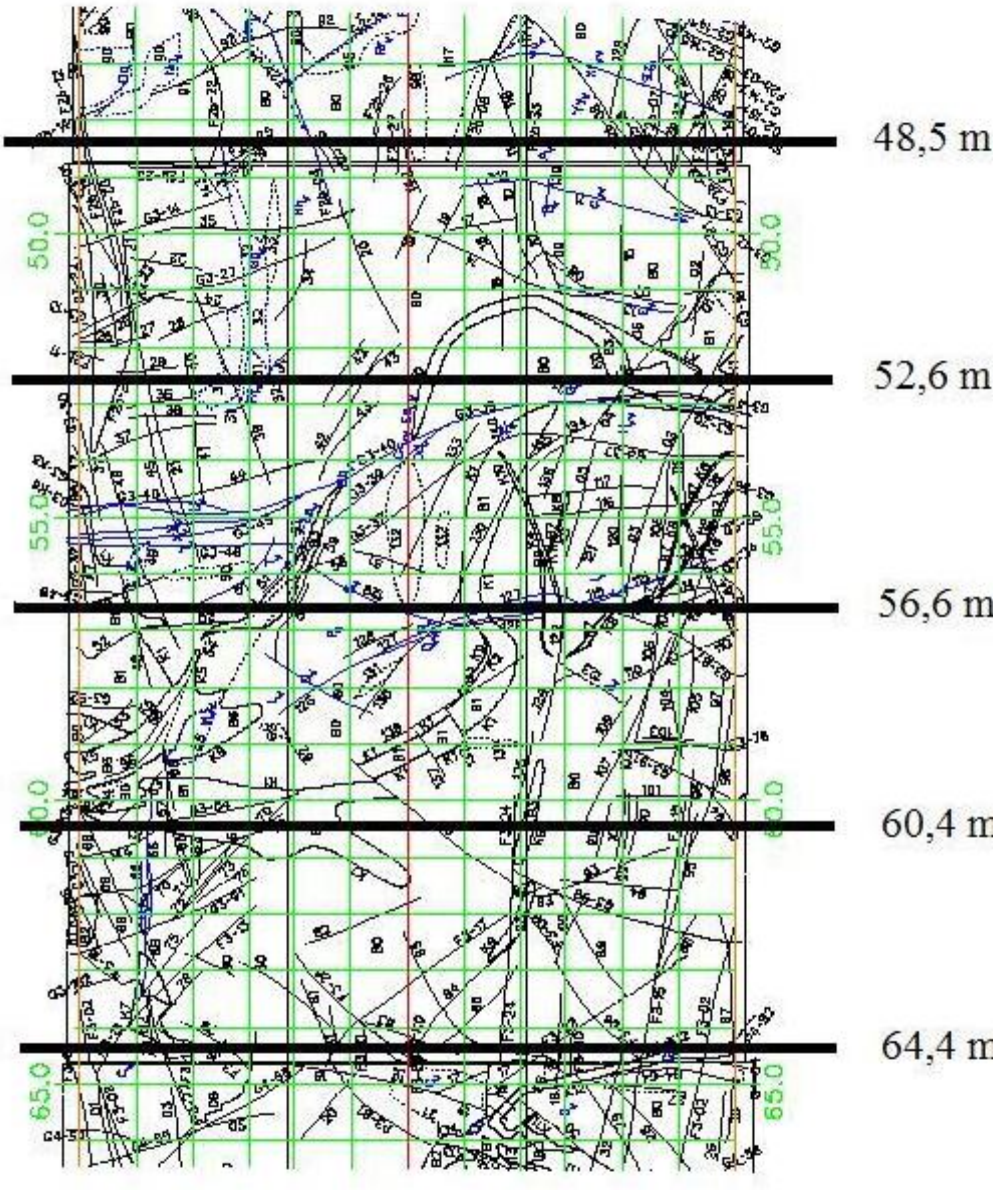

Figure A3: Geological map walls and roof section 47 to 66 m. Modified from Hardenby and Sigurdsson (2010).

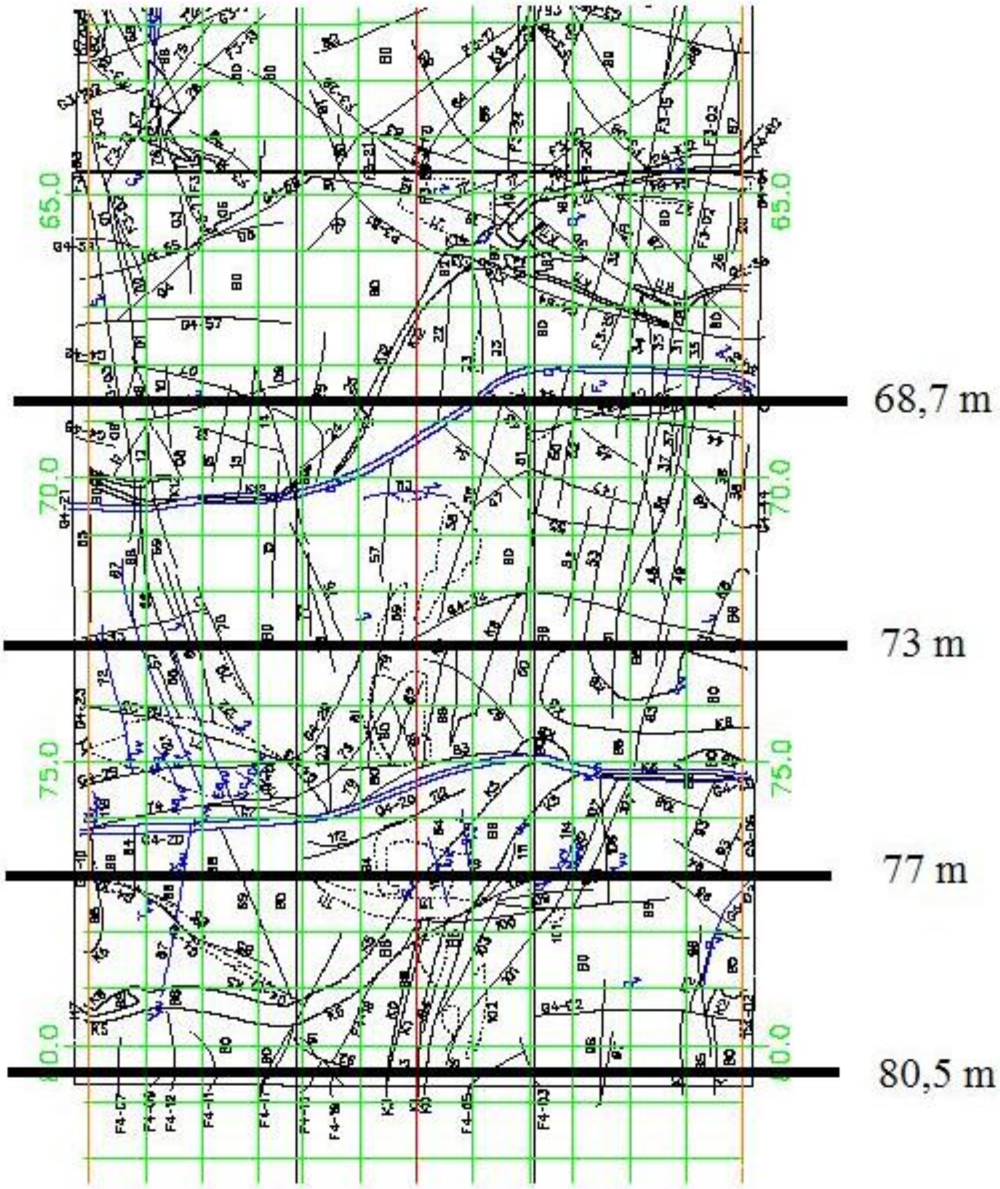

Figure A4: Geological map walls and roof section 62 to 80, 6 m. Modified from Hardenby and Sigurdsson (2010).

Appendix A

B Stress simulations

This appendix contains the results from the numerical stress simulations. The left figures depicts the distribution of secondary or induced principal stress σ_1, resulting from the in situ stress σ_{h1}, 0,001 m in the rock mass from the excavation boundary. The right figures shows the distribution of secondary or induced principal stress σ_1 in the roof of the same section. Including the theoretical section, the stress distribution in 16 sections has been simulated.

The distribution in the right figures are presented in the opposite heading in relation to the left figures, i.e. the tunnel is displayed heading in the opposite direction.

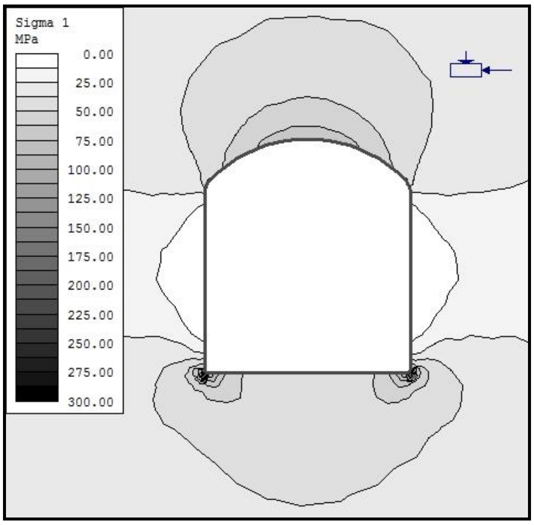

Figure B1: Distribution of secondary stress (σ_1) calculated for the theoretical profile.

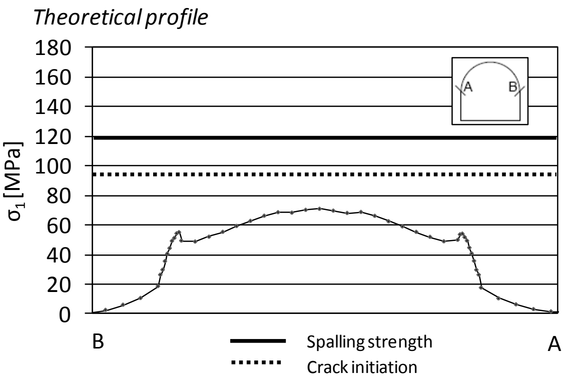

Figure B2: Distribution of secondary stress (σ_1) in the roof of the theoretical section. Crack initiation limit and spalling strength are indicated in the figure.

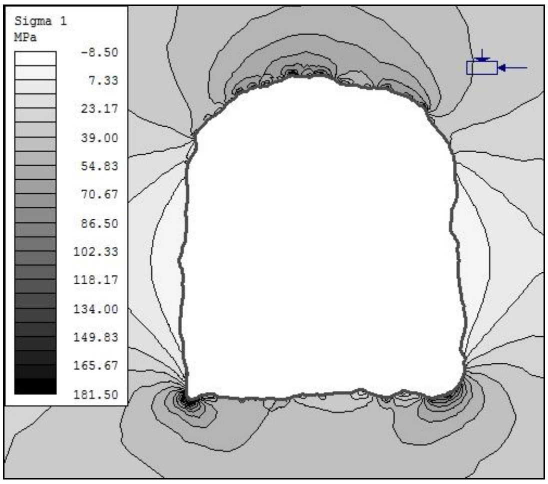

Figure B3: Distribution of secondary stress (σ_1) calculated for the section 24,7 m.

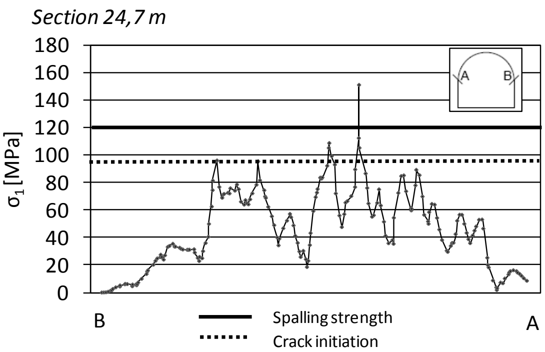

Figure B4: Distribution of secondary stress (σ_1) in the roof of the section 24,7 m. Crack initiation limit and spalling strength are indicated in the figure.

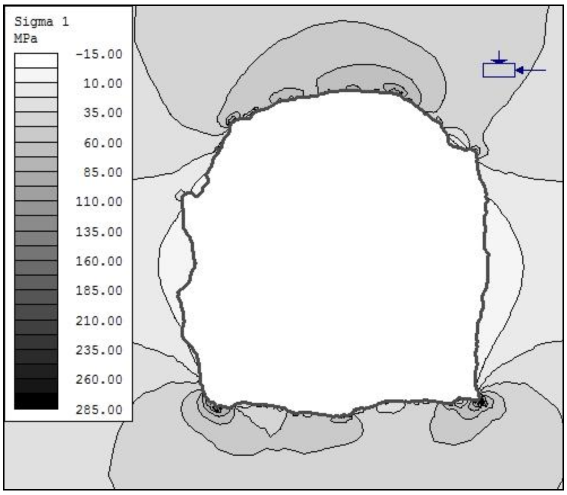

Figure B5: Distribution of secondary stress (σ_1) calculated for the section 28,8 m.

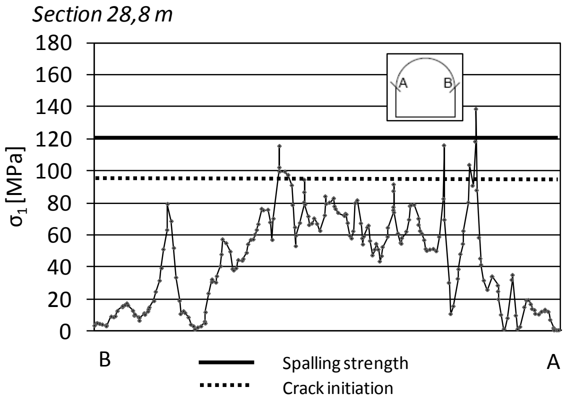

Figure B6: Distribution of secondary stress (σ_1) in the roof of the section 28,8 m. Crack initiation limit and spalling strength are indicated in the figure.

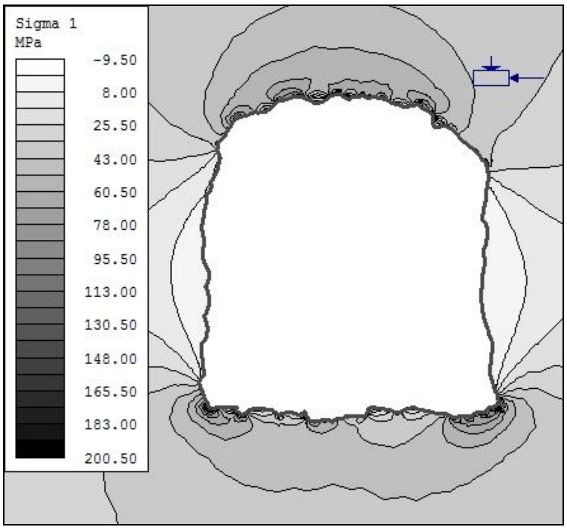

Figure B7: Distribution of secondary stress (σ_1) calculated for the section 32,8 m.

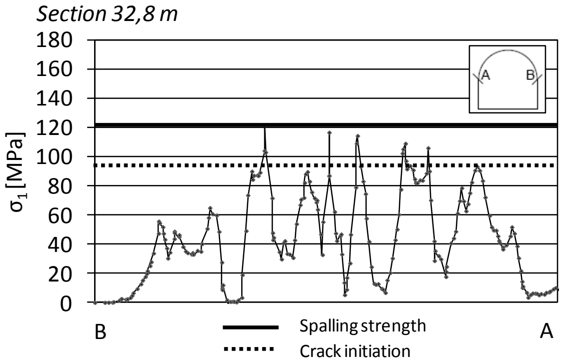

Figure B8: Distribution of secondary stress (σ_1) in the roof of the section 32,2 m. Crack initiation limit and spalling strength are indicated in the figure.

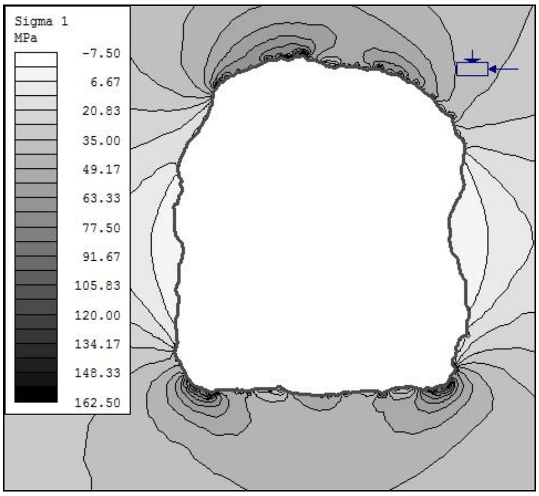

Figure B9: Distribution of secondary stress (σ_1) calculated for the section 37,3 m.

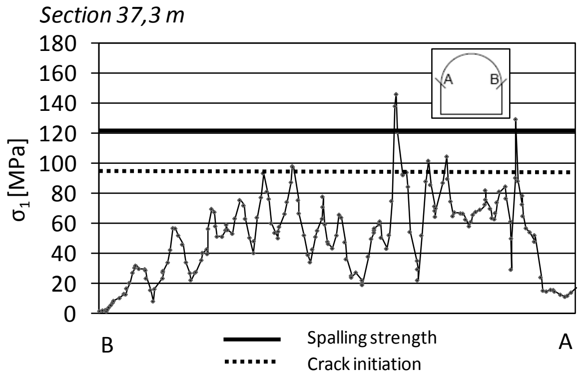

Figure B10: Distribution of secondary stress (σ_1) in the roof of the section 37,3 m. Crack initiation limit and spalling strength are indicated in the figure.

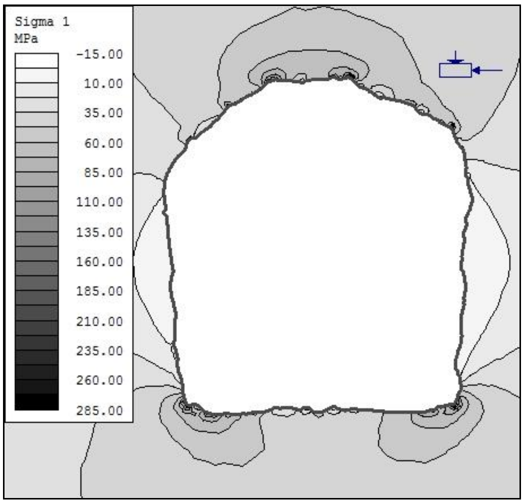

Figure B11: Distribution of secondary stress (σ_1) calculated for the section 42 m.

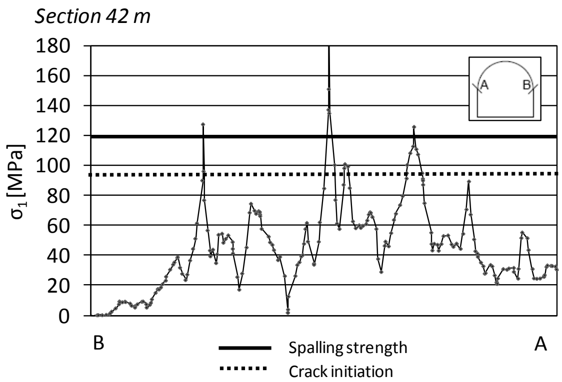

Figure B12: Distribution of secondary stress (σ_1) in the roof of the section 42 m. Crack initiation limit and spalling strength are indicated in the figure.

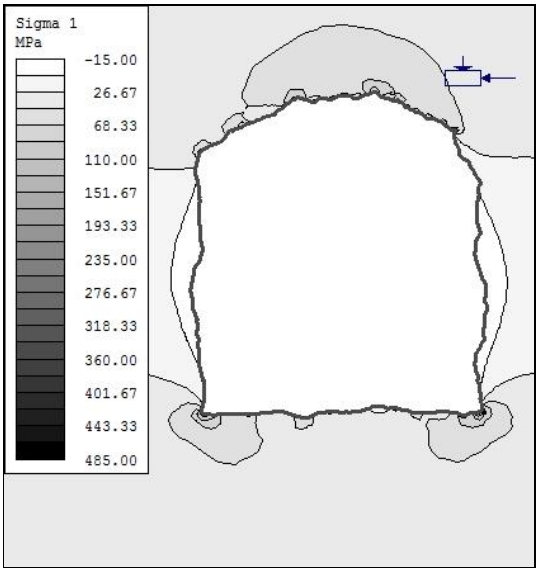

Figure B13: Distribution of secondary stress (σ_1) calculated for the section 45,6 m.

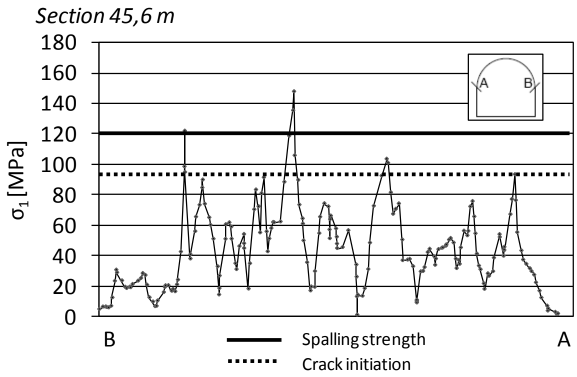

Figure B14: Distribution of secondary stress (σ_1) in the roof of the section 45,6 m. Crack initiation limit and spalling strength are indicated in the figure.

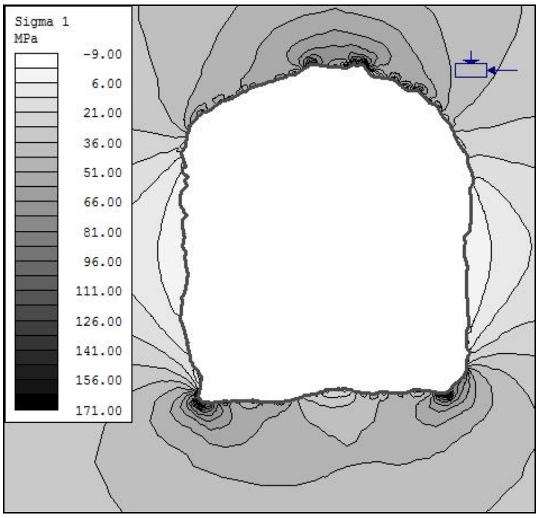

Figure B15: Distribution of secondary stress (σ_1) calculated for the section 48,5 m.

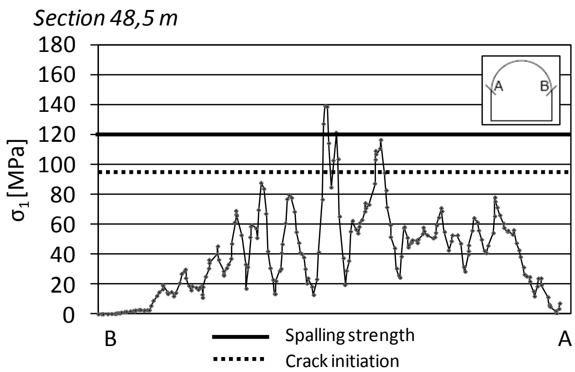

Figure B16: Distribution of secondary stress (σ_1) in the roof of the section 48,5 m. Crack initiation limit and spalling strength are indicated in the figure.

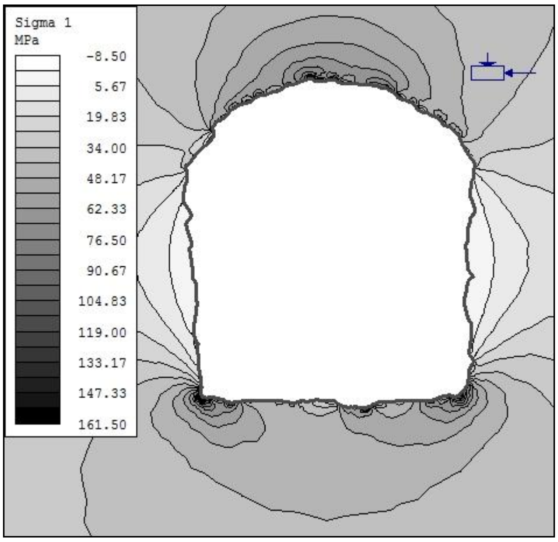

Figure B17: Distribution of secondary stress (σ_1) calculated for the section 52,6 m.

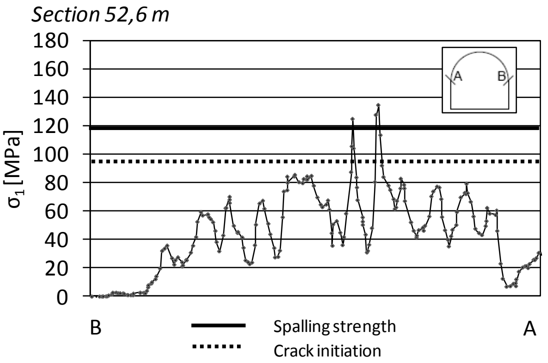

Figure B18: Distribution of secondary stress (σ_1) in the roof of the section 52,6 m. Crack initiation limit and spalling strength are indicated in the figure.

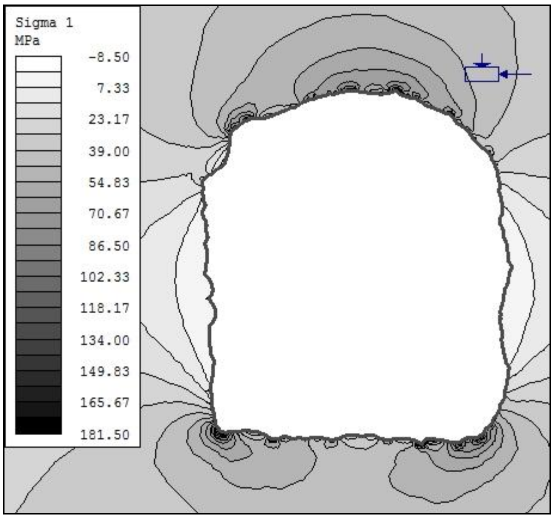

Figure B19: Distribution of secondary stress (σ_1) calculated for the section 56,6 m.

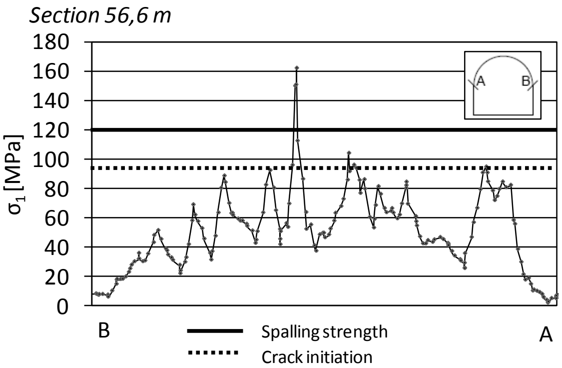

Figure B20: Distribution of secondary stress (σ_1) in the roof of the section 56,6 m. Crack initiation limit and spalling strength are indicated in the figure.

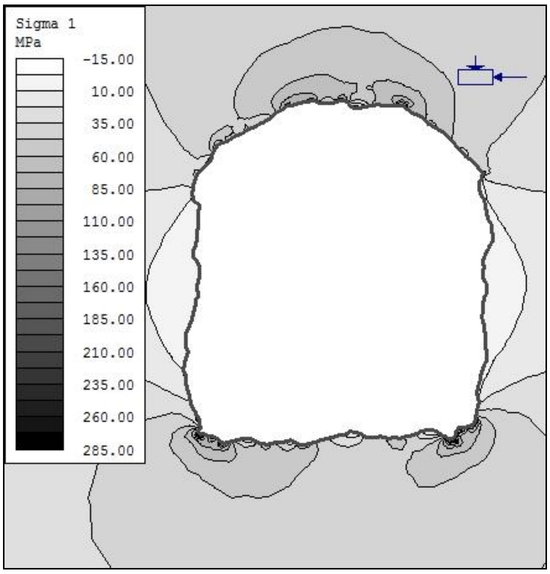

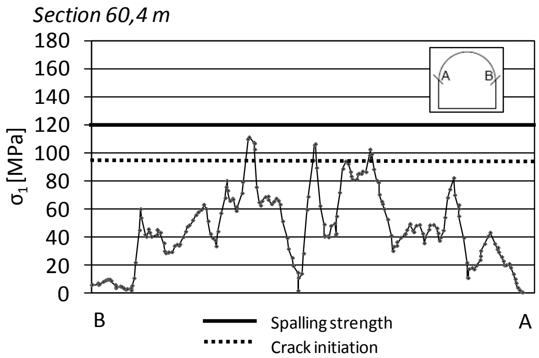

Figure B21: Distribution of secondary stress (σ_1) calculated for the section 60,4 m.

Figure B22: Distribution of secondary stress (σ_1) in the roof of the section 60,4 m. Crack initiation limit and spalling strength are indicated in the figure.

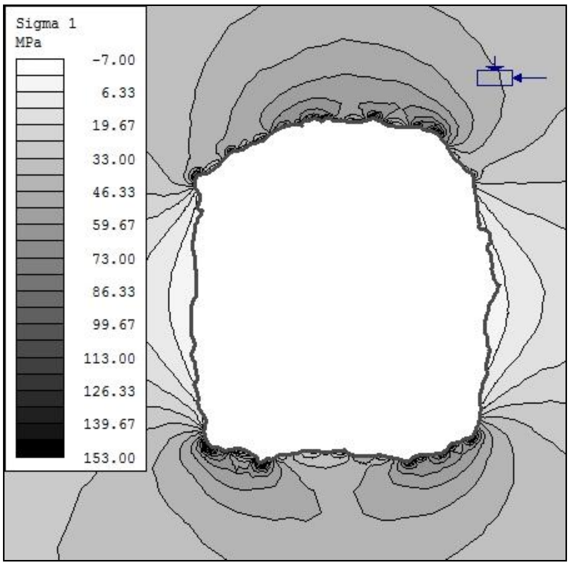

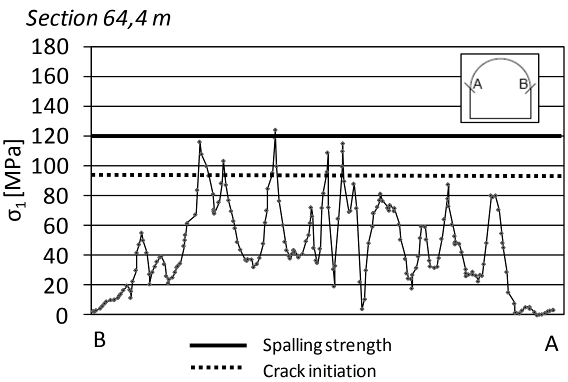

Figure B23: Distribution of secondary stress (σ_1) calculated for the section 64,4 m.

Figure B24: Distribution of secondary stress (σ_1) in the roof of the section 64,4 m. Crack initiation limit and spalling strength are indicated in the figure.

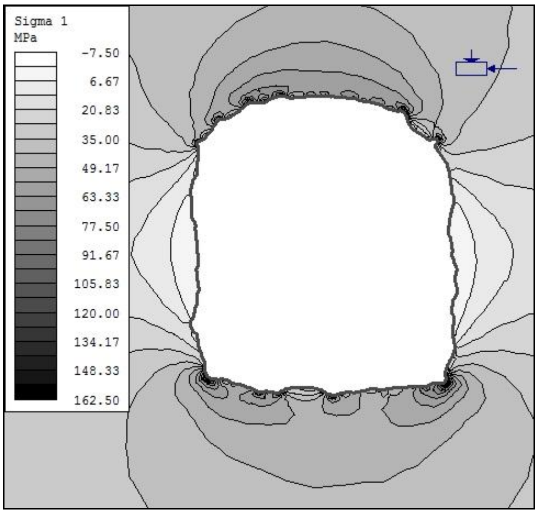

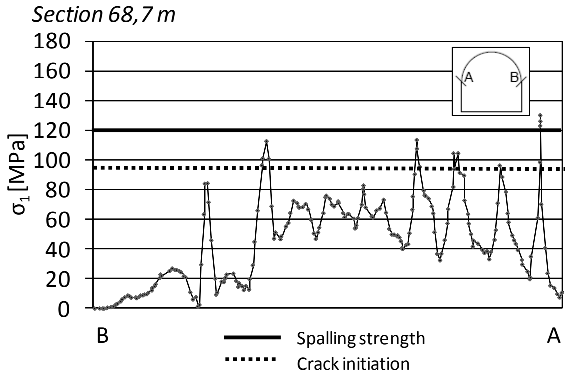

Figure B25: Distribution of secondary stress (σ_1) calculated for the section 68,7 m.

Figure B26: Distribution of secondary stress (σ_1) in the roof of the section 68,7. Crack initiation limit and spalling strength are indicated in the figure.

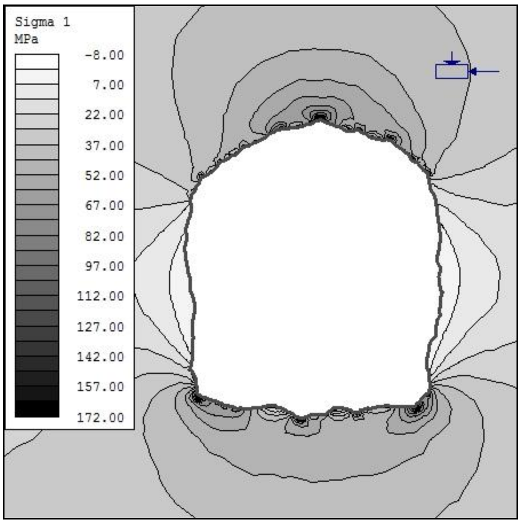

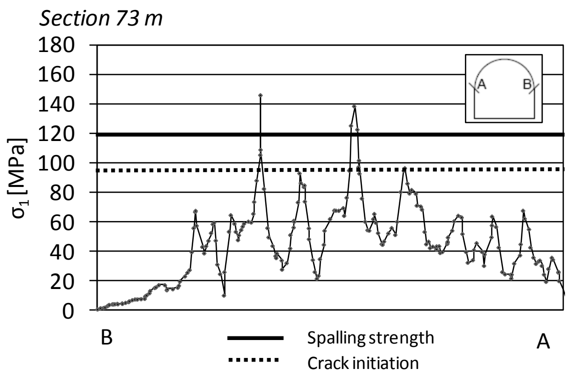

Figure B27: Distribution of secondary stress (σ_1) calculated for the section 73 m.

Figure B28: Distribution of secondary stress (σ_1) in the roof of the section 73 m. Crack initiation limit and spalling strength are indicated in the figure.

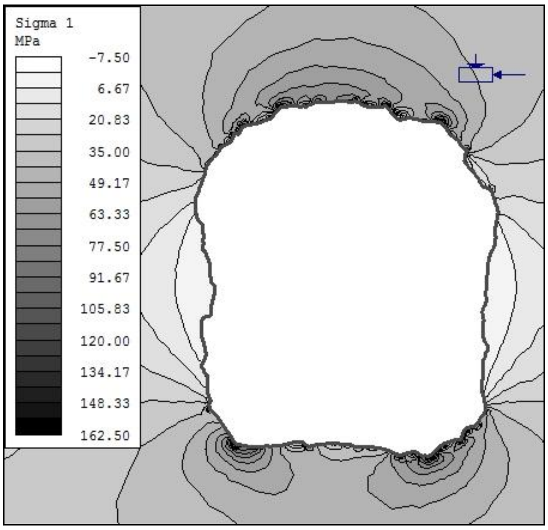

Figure B29: Distribution of secondary stress (σ_1) calculated for the section 77 m.

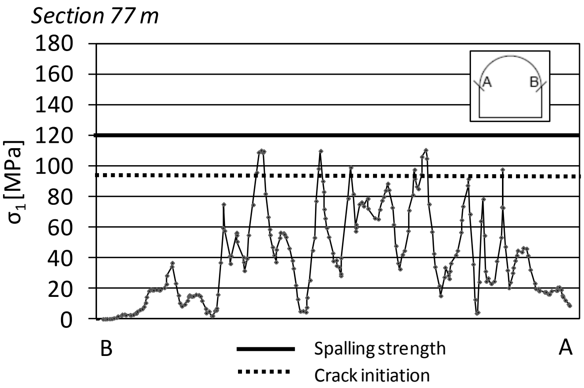

Figure B30: Distribution of secondary stress (σ_1) in the roof of the section 77 m. Crack initiation limit and spalling strength are indicated in the figure.

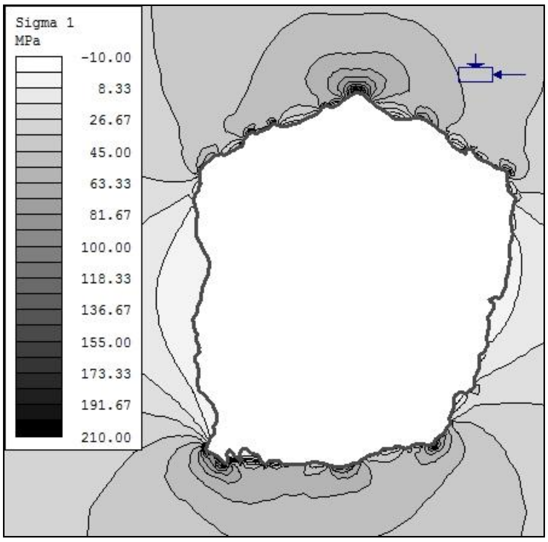

Figure B31: Distribution of secondary stress (σ_1) calculated for the section 80,5 m.

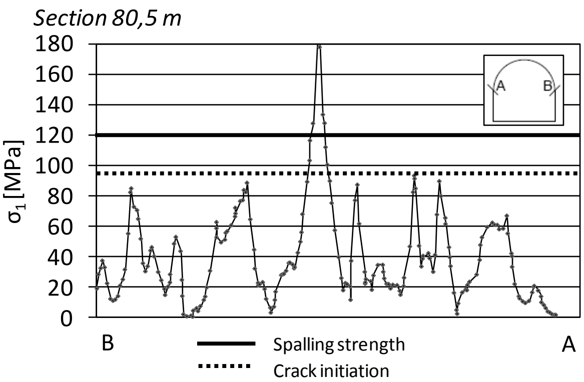

Figure B32: Distribution of secondary stress (σ_1) in the roof of the section 80,5m. Crack initiation limit and spalling strength are indicated in the figure.

Appendix B

C Support capacity

This appendix contains the calculations of support capacities.

C.1 Spray concrete

C.2 Chain linked wire mesh

C.3 Welded wire mesh

C.1 Spray concrete

Spray concrete adhesion:

$\text{Fad1} := 0.8 \cdot \text{MPa} \qquad \text{Fad2} := 1.5 \cdot \text{MPa} \qquad \delta := 0.003 \cdot \text{m}$

Load on spray conctrete:

Mean block:	Median block:
$\text{Mean} := 182 \cdot \text{kg}$	$\text{Median} := 86 \cdot \text{kg}$
$\text{Lmean} := 0.509 \cdot \text{m}$	$\text{Lmedian} := 0.422 \cdot \text{m}$

$$\text{qmean} := \frac{\text{Mean} \cdot g}{\text{Lmean}^2} \qquad \text{qmedian} := \frac{\text{Median} \cdot g}{\text{Lmedian}^2}$$

Required adhesion strength for the mean block:

$$\sigma\text{admean} := \text{qmean} \cdot \frac{\text{Lmean}}{2\delta} = 5.844 \times 10^5 \,\text{Pa}$$

Required adhesion strength for the median block:

$$\sigma\text{admedian} := \text{qmedian} \cdot \frac{\text{Lmedian}}{2\delta} = 3.331 \times 10^5 \,\text{Pa}$$

Factors of safety:

$$\text{FS1mean} := \frac{\text{Fad1}}{\sigma\text{admean}} = 1.369 \qquad \text{FS1median} := \frac{\text{Fad1}}{\sigma\text{admedian}} = 2.402$$

$$\text{FS2mean} := \frac{\text{Fad2}}{\sigma\text{admean}} = 2.567 \qquad \text{FS2median} := \frac{\text{Fad2}}{\sigma\text{admedian}} = 4.503$$

C.2 Chain linked wire mesh

Loads on chain linked wire mesh:

Mean block:

$Lmean := 0.509 \cdot m$

$Mean := 182 \cdot kg$

Median block:

$Lmedian := 0.422 \cdot m$

$Median := 86 \cdot kg$

Material parameters

$\sigma t := 450 \cdot 10^{6} \cdot Pa \quad t := 0.003 \cdot m \quad aperture := 0.05 \cdot m$

$$A := \pi \cdot \left(\frac{t}{2}\right)^{2} = 7.069 \times 10^{-6} m^{2}$$

$$Nmean := 2 \cdot \frac{Lmean}{aperture} = 20 \qquad Nmedian := 2 \cdot \frac{Lmedian}{aperture} = 17$$

Mesh capacity mean block:

$Fmean := Nmean \cdot A \cdot \sigma t = 6.476 \times 10^{4} N$

Mesh capacity median block:

$Fmedian := Nmedian \cdot A \cdot \sigma t = 5.369 \times 10^{4} N$

Load on mesh mean block

$qmean := (Mean \cdot g) = 1.785 \times 10^{3} N$

Load on mesh median block

$qmedian := (Median \cdot g) = 843.372 N$

$$FSmean := \frac{Fmean}{qmean} = 36.285 \qquad FSmedian := \frac{Fmedian}{qmedian} = 63.665$$

C3: Welded wire mesh

Loads on welded wire mesh:

Mean block:

$Lmean := 0.509 \cdot m$

$Mean := 182 \cdot kg$

Median block:

$Lmedian := 0.422 \cdot m$

$Median := 86 \cdot kg$

Material parameters:

$\sigma t := 555 \cdot 10^{6} \cdot Pa \quad t := 0.006 \cdot m \quad aperture := 0.1 \cdot m$

$$A := \pi \cdot \left(\frac{t}{2}\right)^{2} = 3 \times 10^{-5} m^{2}$$

$$Nmean := 2 \cdot \frac{Lmean}{aperture} = 10 \qquad Nmedian := 2 \cdot \frac{Lmedian}{aperture} = 8$$

Mesh capacity mean block:

$Fmean := Nmean \cdot A \cdot \sigma t = 1.597 \times 10^{5} N$

Mesh capacity median block:

$Fmedian := Nmedian \cdot A \cdot \sigma t = 1.324 \times 10^{5} N$

Load on mesh mean block:

$qmean := (Mean \cdot g) = 1.785 \times 10^{3} N$

Load on mesh median block:

$qmedian := (Median \cdot g) = 843.372 N$

$$FSmean := \frac{Fmean}{qmean} = 89.504 \qquad FSmedian := \frac{Fmedian}{qmedian} = 157.039$$

D Production times and costs

This appendix contains the results from the field work. Included are the active production times for wire mesh and spray concrete and the production costs based on personal communication with the contractors.

Table D1: Wire mesh production times.

Date (yymmdd)	Time Start (hh:mm)	Time Stop (hh:mm)	Activity	Position along object From (m)	Position along object To (m)
110518	8:20	11:35	Drilling	24	30
110518	13:53	14:53	Drilling	24	30
110518	11:37	14:26	Drilling	32	35
110519	11:42	12:25	Drilling	32	35
110518	14:40	16:44	Drilling	72	75
110519	8:45	9:10	Drilling	72	75
110518	16:48	17:35	Drilling	76	78
110519	8:10	8:43	Drilling	76	78
110523	12:45	12:58	Grouting (21 holes)	76	78
110523	12:59	13:10	Grouting (21 holes)	72	75
110524	08:39	09:16	Installation of wire mesh	76	78
110524	09:25	09:56	Installation of wire mesh	72	75

Table D2: Spray concrete production times.

Date (yymmdd)	Duration [min]	Activity	Position along object	
			From (m)	To (m)
110428	18	Spary concrete	64	67
110502	10	Spary concrete	57	59
110502	7	Spary concrete	39	42
110502	18	Spary concrete	35	39
110503	9	Spary concrete	35	39

Table D3: Spray concrete production costs based on personal communication with the contractor.

Machinery	Cost
Platform [SEK/h]	262,5
Drill rig [SEK/h]	468,75
Materials	
Bolt [SEK/bolt]	239
Cement [SEK/kg]	5,4
Mesh [SEK/m^2]	105
Personnel	
Miner [SEK/h]	525

Table D4: Wire mesh production costs based on personal communication with the contractor.

Machinery	Cost
Spray concrete robot including compressor [SEK/day]	10625
Materials	
Spray concrete including transport[SEK/m^3]	2500
Additive [SEK]	2,5 % of spray concrete volume
Parts	10% of spray concrete cost
Personnel	
Miner [SEK/h]	525
Work Supervisor [SEK/h]	565

E Results from mapping

This appendix contains the results from the mapping conducted in February 2011. Six maps were produced:

1. Geological controlled outbreaks
2. Blast damages
3. Maintenance scaling
4. Deviations in geometry
5. Geology
6. Assigned rock support

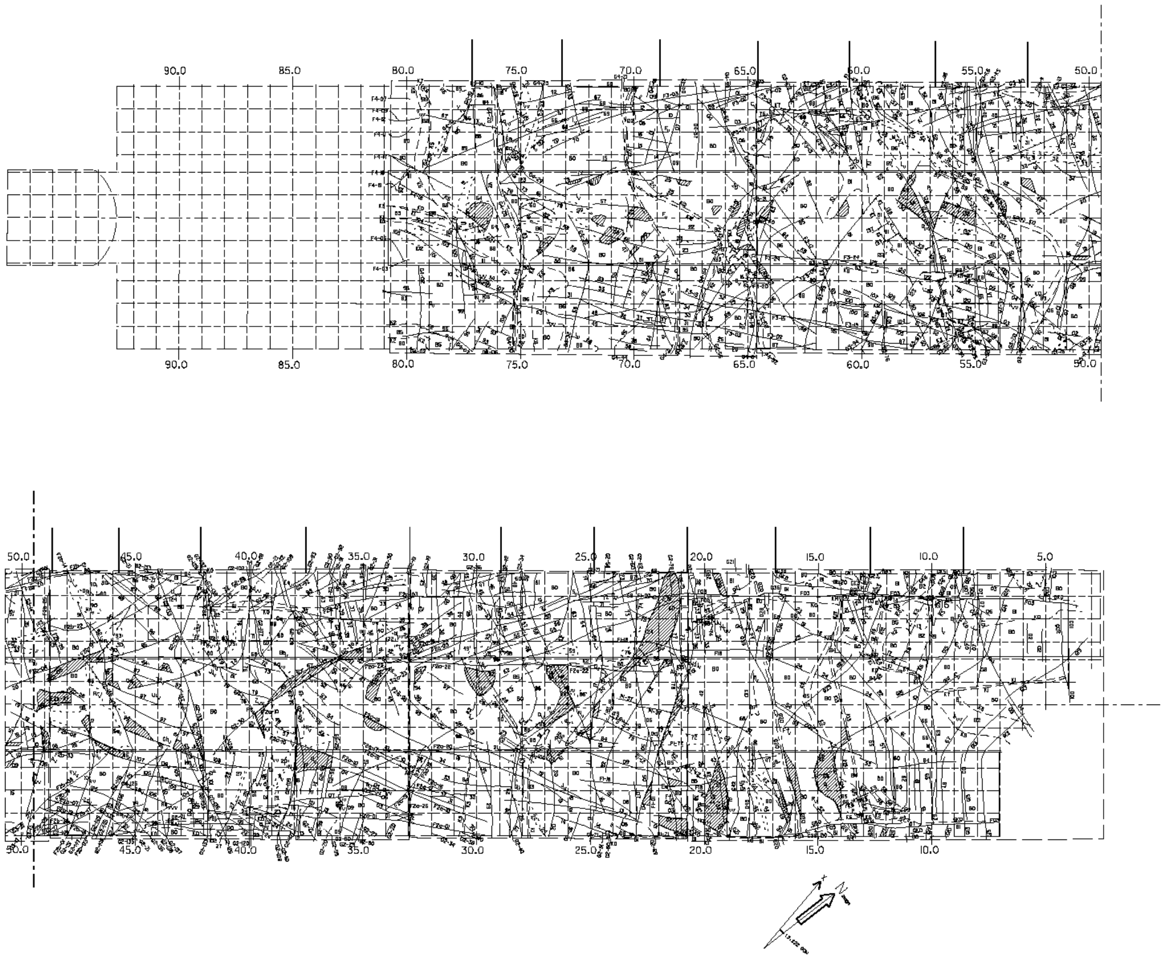

GEOLOGISKT STYRDA BROTT

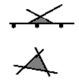

BROTT STYRT
AV SPRICKPLAN
4 ST

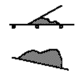

BROTT I INTAKT BERG MOT ETT
ELLER FLERA SPRICKPLAN
64 ST

SKB	PRELIMINÄR 2011-03-07
VATTENFALL POWER CONSULTANT AB	TASS KARTERING BERGUNDERHÅLL GEOLOGISKT STYRDA BROTT SPRÄNGSKADOR MOT SPRICKPLAN –
3221800 | MAYO | –	
–	– | 5033-RITNING 1 | –

ORIGINALFORMAT A1

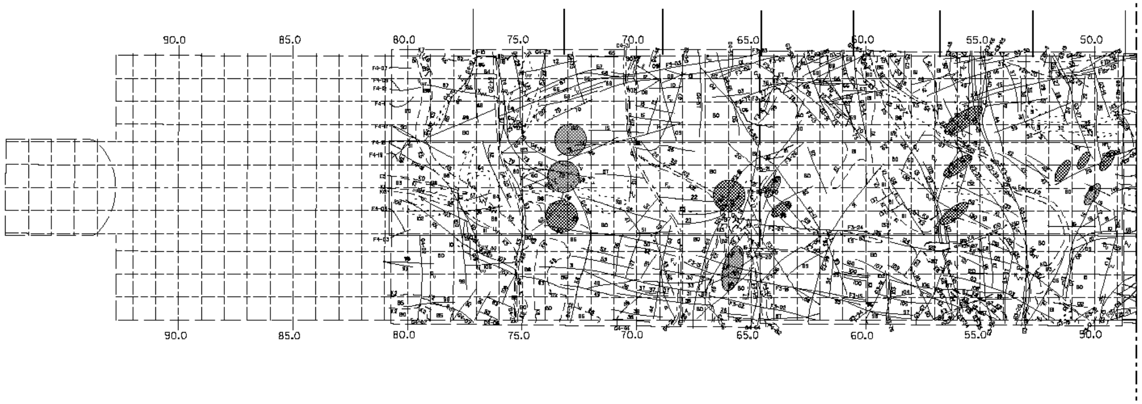

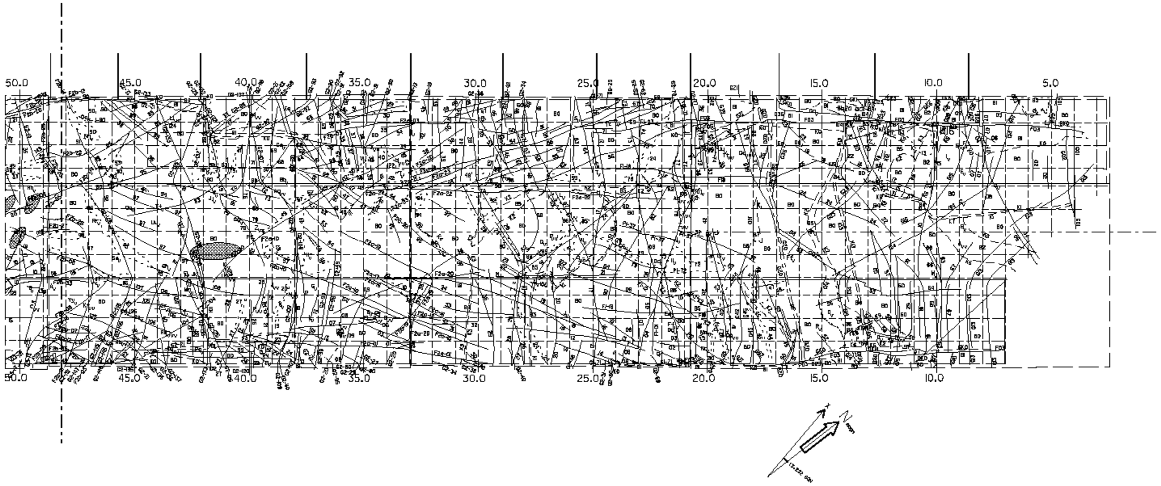

SPRÄNGSKADOR

NORMALT

SPRÄNGSKADAT

SKB	PRELIMINÄR 2011-03-07
VATTENFALL POWER CONSULTANT AB	TASS KARTERING BERGUNDERHÅLL SPRÄNGSKADOR MELLAN BORRHÅL – –
3221800 | MAYO | –	– | 5033-RITNING 2 | –
–	

ORIGINALFORMAT A1

EFTERSKROTNING

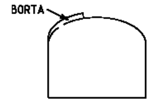

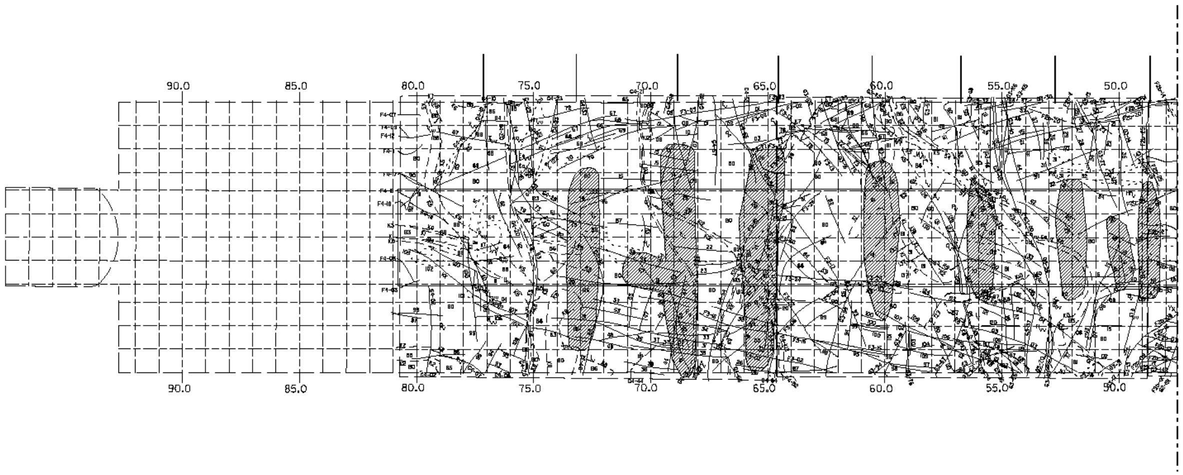

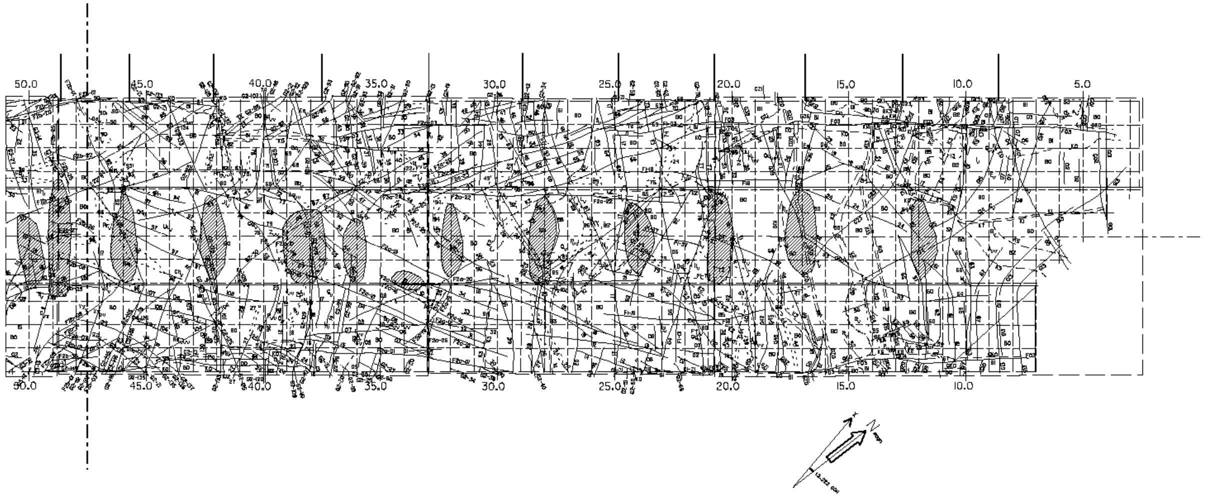

SKB	PRELIMINÄR2011-03-07
VATTENFALL POWER CONSULTANT AB	TASS KARTERING BERGUNDERHÅLL EFTERSKROTNINGSOMRÅDEN SPRICKIGT (SEKUNDÄRA) _
3221800 / MAYO / _	
_	_ / 5033-RITNING 3 / _

ORIGINALFORMAT A1

GEOMETRISKA SKADOR

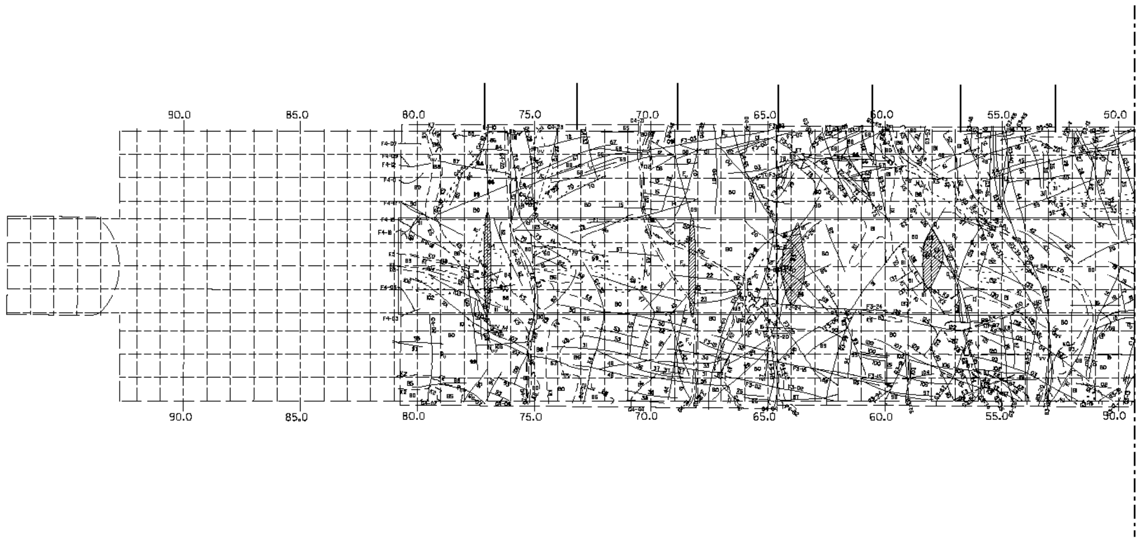

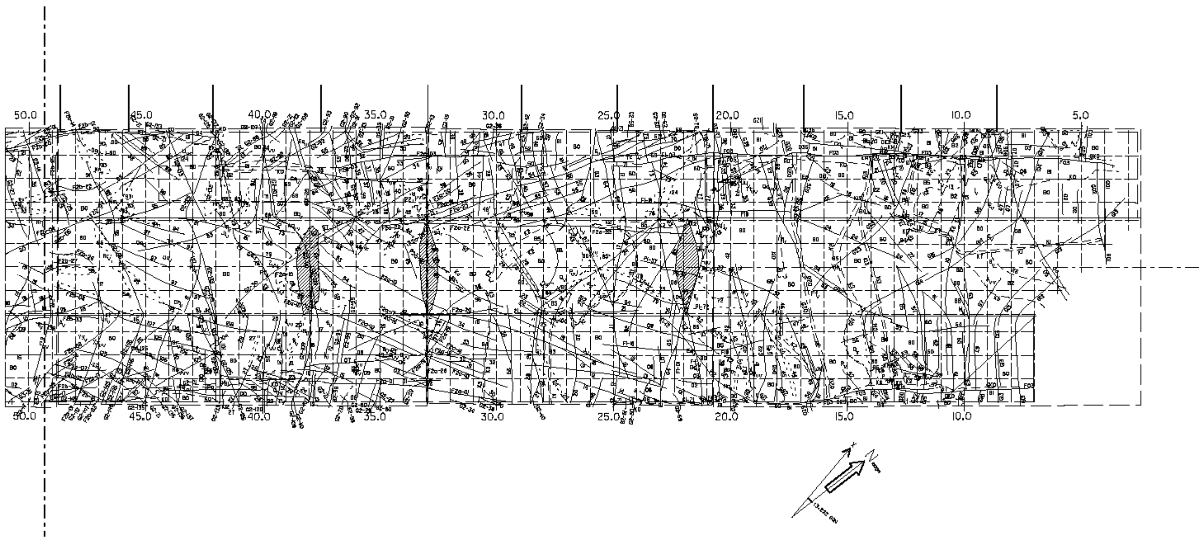

SKB	PRELIMINÄR 2011-03-07
VATTENFALL POWER CONSULTANT AB	TASS KARTERING BERGUNDERHÅLL GEOMETRISKA SKADOR STORA HACK I TAK –
3221800 | MAYO | –	
–	– | 5033-RITNING 4 | –

ORIGINALFORMAT A1

5033-Ritning 4.dgn 2011-03-07 10:10:06

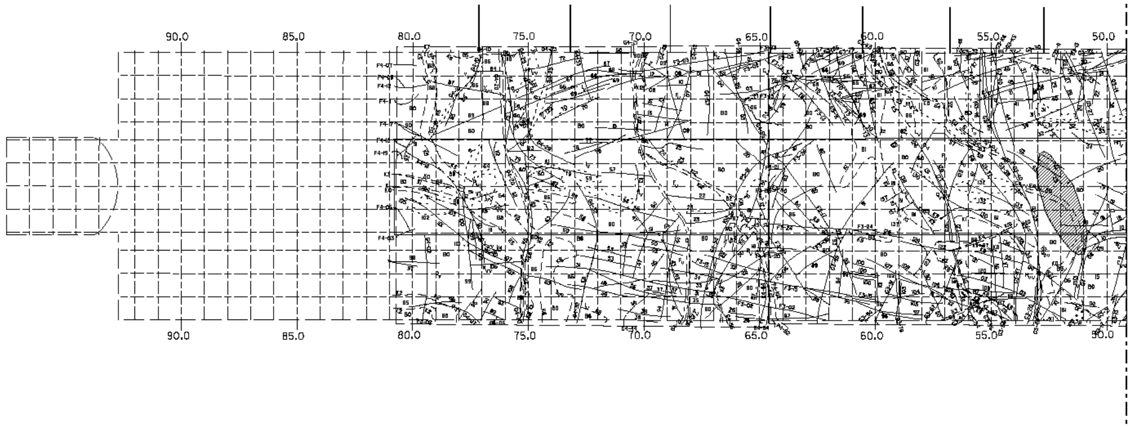

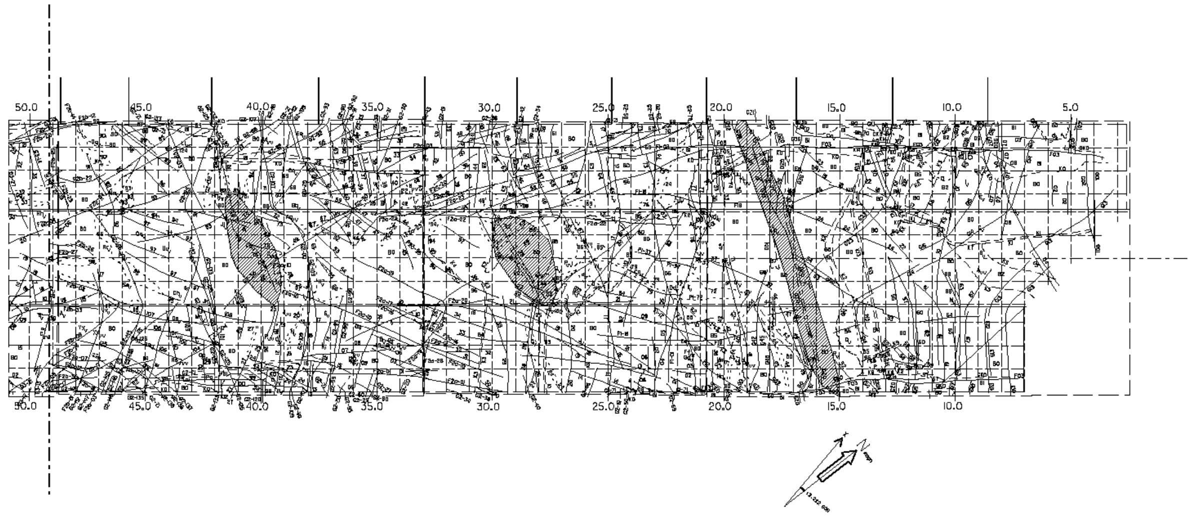

GEOLOGI

OMRÅDEN MED GEOLOGISKT BETINGADE SKADOR
SPRICKIGHET, SKIVOR OCH BLOCK

SKB	PRELIMINÄR 2011-03-07
VATTENFALL POWER CONSULTANT AB	TASS KARTERING BERGUNDERHÅLL GEOLOGISKT BETINGADE SKADOR SPRICKIGHET, SKIVOR OCH BLOCK
3221800 MAYO –	5033-RITNING 5

ORIGINALFORMAT A1

BERGFÖRSTÄRKNING

NÄT

SPRUTBETONG EV. TJOCKARE

SPRUTBETONG

EFTERSKROTNING UTFÖRES DÄR INGEN BERGFÖRSTÄRKNING GJORTS.

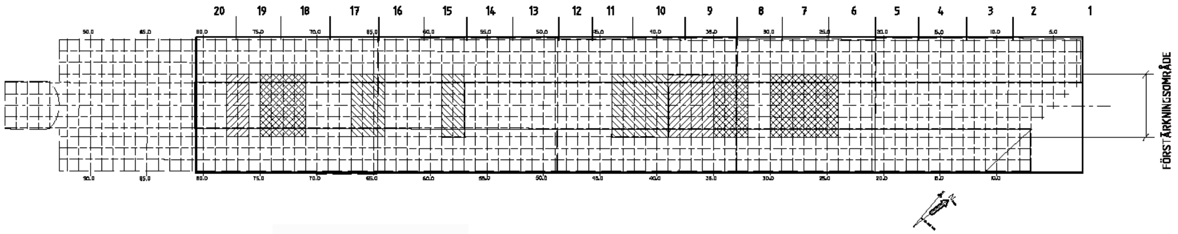

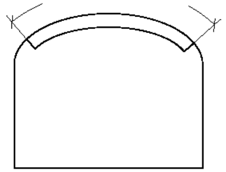

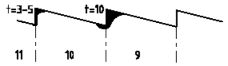

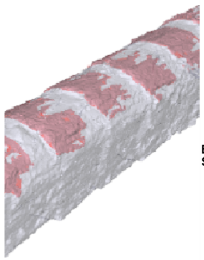

EXEMPEL PÅ UTKILAD SPRUTBETONG VID SALVSLUT

SKB

VATTENFALL POWER CONSULTANT AB

3221800	MAYO	_

PRELIMINÄR 2011-03-07

TASS
KARTERING BERGUNDERHÅLL
FÖRSLAG TILL BERGFÖRSTÄRKNING

5033-RITNING 6

ORIGINALFORMAT A1